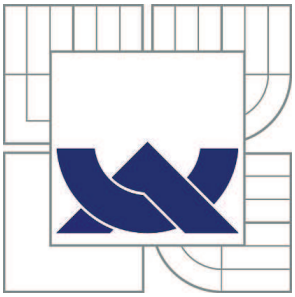

VYSOKÉ UČENÍ TECHNICKÉ V BRNĚ

BRNO UNIVERSITY OF TECHNOLOGY

FAKULTA STROJNÍHO INŽENÝRSTVÍ
ÚSTAV PROCESNÍHO A EKOLOGICKÉHO INŽENÝRSTVÍ

FACULTY OF MECHANICAL ENGINEERING
INSTITUTE OF PROCESS AND ENVIRONMENTAL ENGINEERING

MODELOVÁNÍ PROUDĚNÍ V ZAŘÍZENÍCH PROCESNÍHO PRŮMYSLU

FLOW MODELLING FOR APPLICATIONS IN PROCESS INDUSTRY

DIPLOMOVÁ PRÁCE
MASTER'S THESIS

AUTOR PRÁCE — Bc. MICHAL BIALOŽYT
AUTHOR

VEDOUCÍ PRÁCE — doc. Ing. JIŘÍ HÁJEK, Ph.D.
SUPERVISOR

BRNO 2012

Vysoké učení technické v Brně, Fakulta strojního inženýrství

Ústav procesního a ekologického inženýrství
Akademický rok: 2011/2012

ZADÁNÍ DIPLOMOVÉ PRÁCE

student(ka): Bc. Michal Bialožyt

který/která studuje v **magisterském navazujícím studijním programu**

obor: **Procesní inženýrství (3909T003)**

Ředitel ústavu Vám v souladu se zákonem č.111/1998 o vysokých školách a se Studijním a zkušebním řádem VUT v Brně určuje následující téma diplomové práce:

Modelování proudění v zařízeních procesního průmyslu

v anglickém jazyce:

Flow modelling for applications in process industry

Stručná charakteristika problematiky úkolu:

Při modelování proudění a přestupu tepla v zařízeních procesního průmyslu, jako jsou výměníky tepla a spalovací komory, je nutné často přistoupit ke zjednodušení uvažované geometrie. Otázkou však je jak takové zjednodušení ovlivňuje výpočet. Jedním příkladem může být nahrazení dlouhé trubky výměníku trubkou kratší se zařazenou porézní vrstvou.

Cíle diplomové práce:

Cílem bude vytvořit několik modelů potrubí s porézní vrstvou a bez ní, na kterých se otestuje vliv takovéto vrstvy na proudění, tlakovou ztrátu a na přestup tepla. Po určení vhodných parametrů porézní vrstvy se tato aplikuje na zjednodušený model výměníku tepla. Ve druhé části práce bude předmětem práce spalovací komora. Úkolem bude vyšetřit nezávislost numerického výpočtu na jemnosti sítě. Výsledkem by měl být soubor zásad pro tvorbu zjednodušených modelů zařízení procesního průmyslu, především pak výměníků tepla.

Seznam odborné literatury:

F.P. Incropera and D.P. DeWitt, Introduction to Heat Transfer, John Wiley and Sons, Inc., New York (2002).

Vedoucí diplomové práce: doc. Ing. Jiří Hájek, Ph.D.

Termín odevzdání diplomové práce je stanoven časovým plánem akademického roku 2011/2012.

V Brně, dne 21.11.2011

L.S.

_____	_____
prof. Ing. Petr Stehlík, CSc.	prof. RNDr. Miroslav Doupovec, CSc., dr. h. c.
Ředitel ústavu	Děkan fakulty

Abstrakt

Tato diplomová práce se zabývá vlivem zjednodušené geometrie na výpočet pomocí počítačového modelování proudění. Konkrétně se jedná o možnost náhrady části trubky porézní vrstvou, která má odpovídající tlakovou ztrátu jako nahrazený úsek. Řešen je také přestup tepla a jeho vliv na proudění a tlakovou ztrátu. Jako nejúčinnější řešení se ukázalo zakomponování vlivu přestupu tepla na tlakovou ztrátu do porézní vrstvy. Toto řešení nevyžaduje použití rovnice energie a je tudíž nejméně výpočetně nákladné. Získané poznatky jsou poté testovány na modelu reálného výměníku tepla, který má problémy se zanášením a distribucí proudu. Náhrada porézní vrstvou se ukázala jako spolehlivé řešení. Dalším bodem práce je testování závislosti výpočtu turbulentního difúzního spalování na jemnosti výpočetní sítě. K tomuto účelu byl využit model spalovací komory. Po prvním výpočtu byla výpočetní síť, na základě výsledků, zjemněna v oblasti vířiče a v oblasti plamene, kde dochází k největším gradientům. Po adaptaci výpočetní sítě bylo dosaženo téměř dvojnásobného počtu buněk a výpočet byl opakován. Výpočet s adaptovanou výpočetní sítí se ukázal být mnohokrát časově náročnější a byl proto zastaven jelikož přesahuje rámec této práce. Předběžné výsledky byly zpracovány.

Abstract

This master thesis is aimed to simplify geometry for the purpose of computational fluid dynamics simulations and its influence on the result. A possibility to replace a part of the heat exchangers tube by a porous zone is examined. The porous zone has the same pressure drop as the missing part. Afterwards the heat transfer and its influence on flow and pressure drop is examined. The most effective is to include the heat transfer effect on the pressure drop directly into the porous zone. This approach does not require to solve energy equation. Therefore it takes less computational power. Gained findings are then applied to the real heat exchanger, which has chocking and distribution problems. The porous zone replacement turn out to be a reliable solution. As the next step there was tested the calculation independence on the mesh quality. Burner test chamber was used for this purpose. The mesh was adapted, based on results, after the first calculation. The mesh was refined in a region of swirl and in a region of flame, where were the biggest gradients. The mesh size was almost doubled after the adaptation and calculation was repeated. The calculation with adapted mesh turned to be very

time demanding and beyond the scope of this thesis. Preliminary results were processed.

Klíčová slova

CFD, porézní vrstva, výměník tepla, výpočetní síť

Key words

CFD, porous zone, heat exchanger, mesh

Citace

BIALOŽYT, M. Modelování proudění v zařízeních procesního průmyslu. Brno: Vysoké učení technické v Brně, Fakulta strojního inženýrství, 2012. XY s. Vedoucí diplomové práce doc. Ing. Jiří Hájek, Ph.D..

Prohlášení

Prohlašuji, že jsem tuto bakalářskou práci vypracoval samostatně pod vedením Ing. Jiřího Vondála

.....
Michal Bialožyt
24. května 2012

Poděkování

Rád bych poděkoval Ing. Jiřímu Vondálovi za profesionální přístup a odborné vedení při tvorbě této práce a Mgr. Petře Brukové za pomoc s anglickou gramatikou. Hlavně by jsem zde ale chtěl poděkovat mé rodině za veškerou podporu během celé doby mého studia.

Obsah

1 Introduction **11**

2 Motivation **12**

3 Porous zone substitution **13**
3.1 Introduction 13
3.2 Briefly about CFD 13
3.3 Theory 15
3.4 Single tube test 16
3.4.1 Porous zone implementation 18
3.4.2 Single tube test results 20
3.5 Mesh influence 22
3.5.1 Mesh influence results 23
3.6 Temperature influence 28
3.6.1 Calculations and settings 28
3.6.2 Geometry 30
3.6.3 Results 31
3.6.4 Other temperature solution 34
3.7 Summary 37

4 Real heat exchanger application **38**
4.1 Pre-calculation processes 39
4.1.1 HX results 40
4.2 Heat exchanger with new diffuser design 47
4.2.1 Results of heat exchanger with new diffuser design 47
4.3 Heat exchanger with new diffuser design and temperature influence 52
4.3.1 Results of heat exchanger with new diffuser design and temperature influence 53
4.4 More precise inertial resistance coefficients for temperature influence 55
4.5 Summary 60

5 Mesh quality influence **61**
5.1 Introduction 61
5.2 Burner test chamber 61
5.3 Mesh and solver settings 62

5.4 Results with basic mesh 64
5.5 Results with adapted mesh 67

6 Conclusions **70**

Nomenclature

Symbol	Meaning	unit
A	cross section area of the tube	m^2
A_i	inner heat transfer area of the tube	m^2
A_o	outer heat transfer area of the tube	m^2
C	prescribed matrix	-
C_g	coefficient for calculation Nusselt number	-
c_p	specific heat	J/kg-K
C_2	inertial resistance coefficient	1/m
D	prescribed matrix	-
D_h	hydraulic diameter	m
D_i	inner diameter	m
D_o	outer diameter	m
f	friction factor	-
f_1	coefficient for calculation local loss coefficient	-
f_2	coefficient for calculation local loss coefficient	-
h_i	inner heat transfer coefficient	W/m^2-K
h_o	outer heat transfer coefficient	W/m^2-K
kr	roughness height	m
k_i	thermal conductivity of the inner flow	W/m-K
k_o	thermal conductivity of the outer flow	W/m-K
k_w	thermal conductivity of the wall	W/m-K
L	length of the tube	m
L_p	length of the porous zone	m
m	coefficient for calculation Nusselt number	-
$\dot{m}$	mass flow rate	kg/s
M	molar weight	mol

m	coefficient for calculation Nusselt number	-
Nu	Nusselt number	-
p	static pressure	Pa
p_a	atmospheric pressure	Pa
Pr	Prandtl number	-
$\dot{q}$	heat flux	W/m^2
r	relative roughness	-
R	universal gas constant	J/K-mol
R_a	radius of bending	m
R_i	thermal resistance of the inner fluid	W/K
R_o	thermal resistance of the outer fluid	W/K
R_w	thermal resistance of the wall	W/K
Re	Reynolds number	-
S	source term	N/m
T	thermodynamic temperature	K
t	temperature	°C
v	velocity	m/s
v_τ	friction velocity	m/s
y	distance from the wall	m

Greek symbol	Meaning	unit
α	permeability	-
δ	thickness of the near wall region	m
λ	D'Arcy-Weisbach friction coefficient	-
μ	dynamic viscosity	Pa-s
ν	kinematic viscosity	m^2/s
ξ	local loss coefficient	-
ρ	density	kg/m^3

1 Introduction

Large heat exchangers are used in a variety of industrial applications. It is usual that heat exchangers are experiencing some flow distribution or fouling problems. These problems can be due to a bad design or a change of process parameters. An experimentation is still the main approach for designing heat exchangers because of the complexity of its flow and heat transfer behaviors. But when there is a need to investigate performance problems, then it is better to use computational fluid dynamics (CFD). The main advantages of CFD are: (1) it is cheaper than experimental testing, (2) it is easy to visualize the flow through the heat exchanger and (3) there is a possibility to do quick changes in a geometry design. Flow in heat exchanger is usually turbulent and there is also the heat transfer, therefore to obtain valid CFD results there is a demand for a fine mesh. However, since the dimensions of the heat exchanger tubes and the flow passages in modern designs are usually very small, the construction of such a mesh can lead to very fine grids with many cells and high demands for CPU power and memory requirements. To cut down the computational cost, the major part of each tube is replaced by a porous zone. There are several papers where the usage of the porous zone is described while modeling heat exchangers. For example Missirlis et al. [1] who investigated the heat transfer and the pressure drop in the heat exchanger for an aero engine application , Shi et al. [2] who introduced a semi-porous media approach for a numerical simulation of the flow through the sparse turbular heat exchanger. Porous zone approach was also used by Wang et al. [3] who investigated flow through fibre membrane bioreactor. The whole tube section is always replaced by porous zone in reviewed literature and the investigation is aimed at an external flow, while this thesis concerns in the internal flow. This thesis introduces concept of replacing major part of heat exchanger tubes with porous zone and mesh quality influence on the results.

2 Motivation

The main motivation is to find computationally manageable and reasonably accurate simplifications of large scale geometries. There are many possible applications e.g. in heat exchanger analysis. Practical case is chocking up of the heat exchanger and its analysis. This heat exchanger is very large and our computational power is not sufficient. Therefore there is a need to find a simplification to be able to calculate this task. The idea is to replace a major part of tubes with porous zone. However we were not able to find any paper which describes using porous zone in specified way. Another big motivation was to find out how mesh quality is influencing CFD results. We would like to know how much accuracy in results we will lose in exchange to possibility of calculation task faster.

3 Porous zone substitution

3.1 Introduction

There is a necessity to calculate the flow through a big heat exchanger (HX). HX usually consist of a geometry, whose purpose is to equally distribute flow (diffuser) to a lot of thin and long tubes. Another flow goes across this tube section and gives or takes heat (depends on a case). Next in order there is geometry which on the other hand gathers the flow from tubes together (collector). This is a basic design concept of tube HX. In a process industry it is usual that this kind of HX is very large and if there is a need to do a computational fluid dynamics (CFD) analysis, then this model has an enormous number of cells and the calculation time is very long. Therefore a simplification is needed to be done to cut down calculation time. One can not afford to make a simplification in geometry of a diffuser or a collector because of complex geometry. The only potential for making simplifications in this case is in the tube section. Tubes have constant diameter. Once the flow profile is developed it will not change until it reaches change in geometry. What can be done is to make tubes shorter but these shorter tubes must have the same pressure drop like their long versions. To achieve this basic assumption, the porous zone, which is usually used to simulate flow through tube banks, filters or packed beds, will be applied.

3.2 Briefly about CFD

Fluid dynamics follows three basic laws which are conservation laws of mass, momentum and energy. This system of conservation laws is called Navier-Stokes equations. However these partial differential equations are very complex and they can not be solved analytically. Therefore numerical solution is used. There are three main numerical discretisation techniques: 1.Finite differential method, 2.Finite element method and 3.Finite volume method. These methods basically divide the whole area of interest into small parts where governing equations are approximated. The solution requires initial and boundary conditions.

The majority of flows in industry are turbulent flows. Turbulent flows are characterized by fluctuating velocity fields. These fluctuations affect transported quantities such as momentum, energy, and species concentration, and cause the transported quantities to fluctuate as well. Turbulence is a very complex phenomenon and to resolve it down to the smallest scales is very computationally costly. Therefore the governing equations have to be manipulated to remove the

resolution of small scales. Two main alternative methods can be employed to render the Navier-Stokes equations. However, the modified equations contain additional unknown variables, and turbulence models are needed to determine these variables in terms of known quantities. The first method is Reynolds-averageing, which divides the field into mean value (average value) and a fluctuation (departure from mean value). These mean values can be solved, while fluctuations in a form of Reynolds stress have to be modeled. With this approach is possible to use the most popular two equations k-ε and k-ω turbulence models. Both models have some specific variations. There are also other RANS models like Spalart-Allmaras model and Reynolds stress model (RSM). The second method is a large eddy simulation (LES). This method is filters small-scale turbulence fluctuations and large eddies are explicitly computed. This method requires more computational power. Detached eddy simulation (DES) is a combination of this two methods. This method uses RANS models in the near-wall region, while the LES treatment is applied to the separated regions. The idea behind is that there are more small scale eddies near the wall than in the core of turbulent flow. There are no universal turbulence model which can be used in all cases. Each of turbulence models have some pros and cons which has to be considered in every specific case. [4, 5, 6]

CFD is mainly a tool for flow simulation but it can handle additional problems as well. There is a possibility to simulate heat transfer, chemistry, radiation, acoustics, solidification and melting. But we have to remember that each equation is adding more computational cost. [4]

CFD requires a geometry model, which has to be divided into small elements. This is called mesh. Mesh must follow turbulence model specifications. At the same time mesh has to be fine in places where rapid changes in fluid properties are expected due to geometry or other effects like the combustion. The finer mesh is the more computational power is needed.

Nowadays CFD has become powerful tool which helps researchers and engineers. There are available powerful computers and also commercial software packages (Fluent, CFX) or open source softwares (OpenFOAM). There is still a need to do experiments, when designing new product, but CFD can help to lower their cost and save the time. CFD is used in many applications from aerodynamics of cars and planes to weather forecast.

3.3 Theory

The porous zone model adds momentum sink in the governing momentum equations. The source term is composed of two parts: a viscous loss term (Darcy, the first term on the right-hand side of Eq. (1)) , and an inertial loss term (the second term on the right-hand side of Eq. (1)). [4]

$$S_i = -\left(\sum_{j=1}^{3} D_{ij}\mu v_j + \sum_{j=1}^{3} C_{ij}\frac{1}{2}\rho \mid v \mid v_j\right) \tag{1}$$

Where S_i is the source term for the i-th (x ,y or z) momentum equation, v is the magnitude of the velocity and D and C are prescribed matrices. This momentum sink contributes to the pressure gradient in the porous cell, creating a pressure drop that is proportional to the fluid velocity (or velocity squared) in the cell. Eq. (2) is simplified Eq. (1) in a case of homogeneous porous media, where α is the permeability and C_2 is the inertial resistance factor, simply specify D and C as diagonal matrices, when D=1/ α and C=C_2. [4]

$$S_i = -\left(\frac{1}{\alpha}\mu v_i + C_2\frac{1}{2}\rho v_i^2\right) \tag{2}$$

At high flow velocities, the constant α is equal to zero and the constant C_2 provides a correction for inertial losses in the porous medium. This constant can be viewed as a loss coefficient per unit length along the flow direction, thereby allowing the pressure drop to be specified as a function of dynamic head. Simplified version of the momentum equation, relating the pressure drop to the source term, can be expressed as Eq. (3), where L_p is length of porous zone. [4]

$$\triangle p = -S_i \cdot L_p \tag{3}$$

Pressure drop can be also calculated with usage of Weisbach formula (4), where ξ is local loss coefficient, ρ is density and v is velocity. The local loss coefficient can be also expressed in a way of using D'Arcy-Weisbach friction coefficient λ, length of tube L and hydraulic diameter D_h. D'Arcy-Weisbach friction coefficient λ depends on flow regime and can be calculated or determined by Moody Diagram. Comparing Eq. (3) to Eq. (4) yields to Eq. (5) for calculating inertial resistance coefficient C_2.

$$\triangle p = \sum_{j=1}^{n}\left(\xi_j \rho \frac{v_j^2}{2}\right) = \sum_{j}^{n}\left(\lambda_j \rho \frac{L_j}{D_{hj}} \cdot \frac{v_j^2}{2}\right) \tag{4}$$

$$-S_i \cdot L_p = \lambda \rho \frac{L}{D_h} \cdot \frac{v^2}{2}$$

$$C_2 \frac{1}{2} \rho v^2 L_p = \lambda \rho \frac{L}{D_h} \cdot \frac{v^2}{2}$$

$$C_2 = \frac{\lambda L}{D_h L_p} \tag{5}$$

3.4 Single tube test

To be able to use porous zone approach in a real application, it had to be tested. Tubes in a case of tube HX are usually U-shaped to maximize heat transfer efficiency. So one U-shaped tube from real HX had been taken and modeled. The porous tube is very short and bendings of U-shaped tube will be part of the porous zone. So U-shaped tube was straightened and also modeled. The bending parts were replaced with corresponding straight sections of length which gives the same pressure drop like bendings. For better visualization see Figure 1.

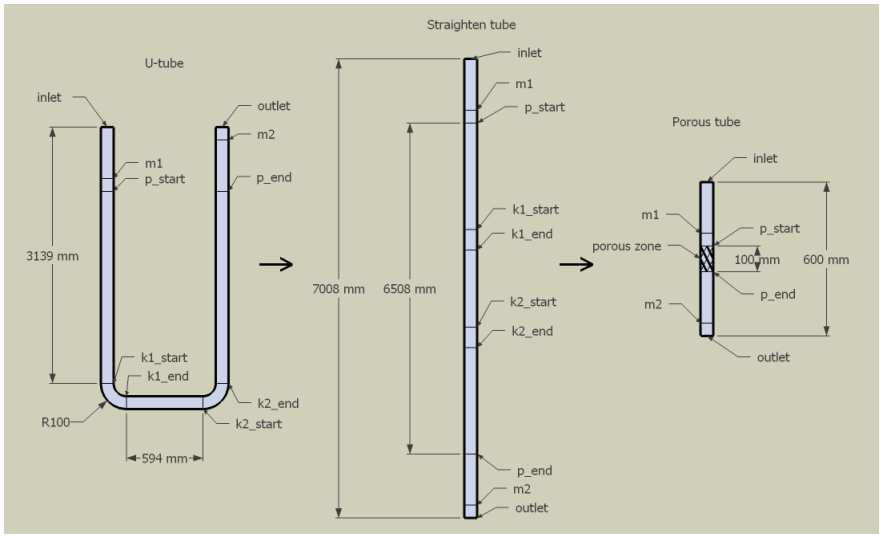

Figure 1: Scheme of porous zone implementation on U-tube

To calculate these corresponding straight sections the modified Weisbach formula (6) was used, where the local loss coef. for bending was determined by Idelchik approach Eq. (7). The flow regime can be determined by Reynolds number Eq. (9), where fluid properties density ρ and viscosity μ are known and mean fluid velocity can be easily calculated according Eq. (8). The turbulence flow regime is expected in a tube so D'Arcy-Weisbach friction coef. λ can be calculated from Nikuradses equation (10), where $k_r$is roughness of the wall. [7, 8]

$$\xi = \lambda \cdot \frac{L}{D_h} \rightarrow L = \frac{\xi \cdot D_h}{\lambda} \tag{6}$$

$$\xi = f_1(\delta) \cdot f_2(R_a/D_h) \tag{7}$$

$$\dot{m} = \rho \cdot v \cdot A \rightarrow v = \frac{\dot{m}}{\rho \cdot A} \tag{8}$$

$$Re = \frac{v\rho D_h}{\mu} \tag{9}$$

$$\lambda = \left[1,14 + 2 \cdot \log\left(\frac{1}{k_r}\right)\right]^{-2} \tag{10}$$

Coefficients $f_1$and f_2 from Eq. (7) were taken from tables 1 and 2. Then there was kept just the first 0.25 m of the straighten tube to allow development of the velocity profile and also the last 0.25 m for the same reason. The remaining length was replaced by the porous zone with the length of just 0.1 m (see Figure 1). An inertial resistance coefficient $C_2$was calculated from this length using Eq. (5).

Table 1: Table for coef. f_1 from Eq. (7) [7]

δ	20	30	45	60	75	90
f_1	0.31	0.45	0.60	0.78	0.90	1

Table 2: Table for coef. f_2 from Eq. (7) [7]

R_a/D_h	0.5	0.6	0.7	0.8	1	1.5	2	4	6	8
f_2	1.18	0.77	0.51	0.37	0.21	0.17	0.15	0.11	0.09	0.07

3.4.1 Porous zone implementation

Three models for just one tube were created in a software Gambit® for comparison. The full length U-tube was modeled, as well as its straighten version and short version with the porous zone (see Figure 1). Geometry and mesh were created in Gambit® as well. Each of the test tube has the same diameter so the same mesh on inlet face was used in each case to achieve identical conditions. In the Figure 2 there is shown an inlet face mesh which was used as a source for meshing the whole volume, on the right side of the Figure 2 can be seen a mesh quality report represented by the green histogram which shows that mesh quality is very good because there is no element with skewness factor higher then 0.4 (0 means good element and 1 is unacceptable). However this mesh is very coarse.

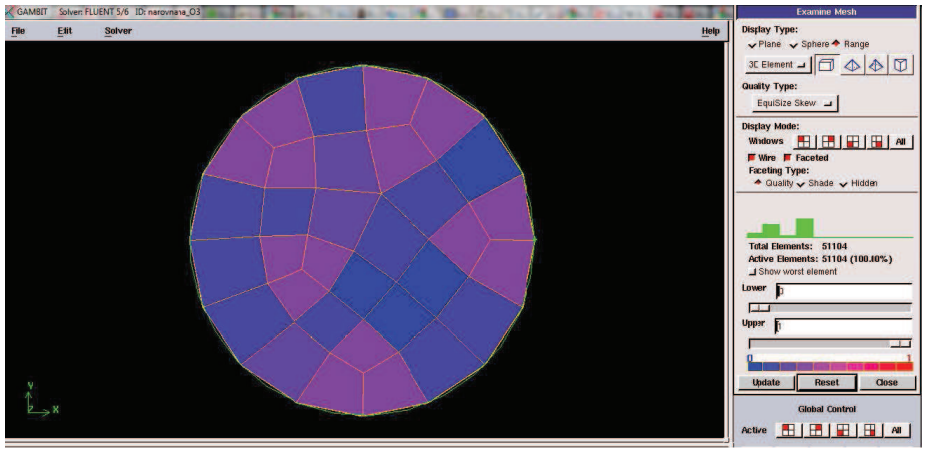

Figure 2: Mesh example and quality

On every model there were created control faces (monitors) in corresponding places to be able to monitor the pressure drop (see Figure 1). Then the task was transferred to Fluent®and identical parameters were set for each case (Table 3). After convergence was reached with the first order upwind discretization scheme. Default convergence setting was switched off and discretization was changed to the second order upwind scheme. Then more iterations were run. Instead of relaying on default convergence criteria, pressure changes in monitors were observed. When there were no more changes and the plot became a constant line (see Figure 3) the convergence was declared.

Table 3: Settings in Fluent®

Turbulent model	SST k-ω
Material of fluid	Process Waste Gas (PWG)
PWG density	0.992 kg/m^3
PWG viscosity	1.62e-5 Pa s
Inlet mass flow rate	0.00427 kg/s
Turbulence intensity at inlet	15 %
Hydraulic diameter	0.0232 m
Wall roughness	0.00025 m
Compute from	inlet
Solution method	SIMPLEC
Skewness correction	1

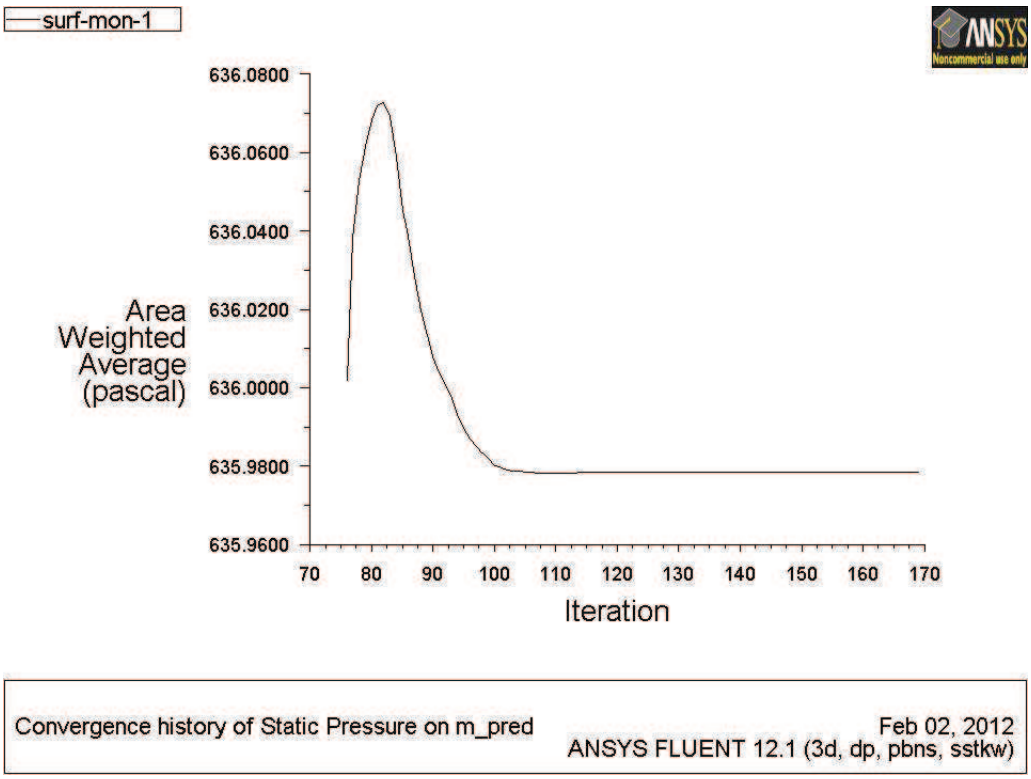

Figure 3: Convergence monitoring

3.4.2 Single tube test results

The results of the comparison test between the U-tube, the straighten tube and the tube with the porous zone are written in Table 4. Also theoretical values calculated with Weisbach Eq. (4) had been added. It can be seen that there is a difference between full-length U-tube and our substitution by the porous zone in a short tube. Figure 4 graphical visualization of Table 4 and on Figure 5 can be seen development of static pressure from inlet to outlet.

Table 4: Static pressure in monitors

	U-pipe	Straighten tube	Porous tube	Theory
inlet [Pa]	691.35	654.79	638.21	609.40
m1 [Pa]	668.41	631.70	615.42	592.18
p_start [Pa]	663.47	627.03	610.72	587.88
p_end [Pa]	23.34	23.17	25.78	21.52
m2 [Pa]	4.83	4.6276	4.91	4.30
outlet [Pa]	0	0	0	0

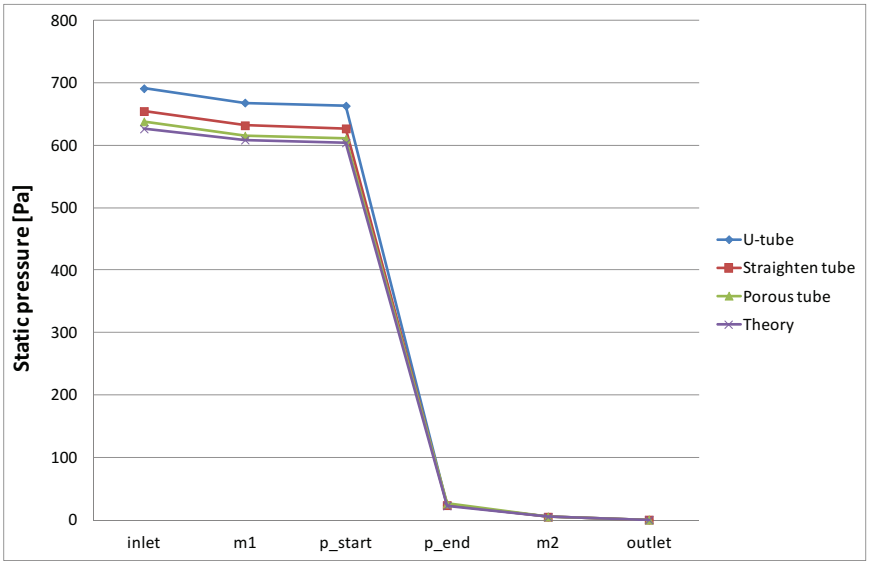

Figure 4: Static pressure in monitors

Figure 5: Static pressure against distance from inlet

As it can be observed in a Table 5 the pressure drop in parts without porous zone is almost identical which is a good sign but the pressure drop in a porous zone itself differs by approximately 10 % between the U-tube and the porous tube but it is just 3% difference between straighten tube and porous tube. And since porous zone coefficient was calculated from straighten tube one can be satisfied with this result. The reason why there is quite a big difference between pressure drop in U-tube and straighten tube can be seen in Table 6. Monitors at the start and at the end of bendings and also at the start and at the end of straight tube, which represents these bendings in straighten tube, shows big difference. In Figure 6 can be observed pressure in the porous tube. Notice development in porous zone.

Table 5: Static pressure drop between monitors

	U-tube	Straighten tube	Porous tube	Theory
inlet - m1 [Pa]	22.94	22.79	22.79	17.22
p_start - p_end [Pa]	640.13	603.86	584.94	566.36

Table 6: Static pressure drop in bending

	U-tube	Straighten tube
k1_start - k1_end [Pa]	19.1	7.7
k2_start - k2_end [Pa]	19.4	6.3

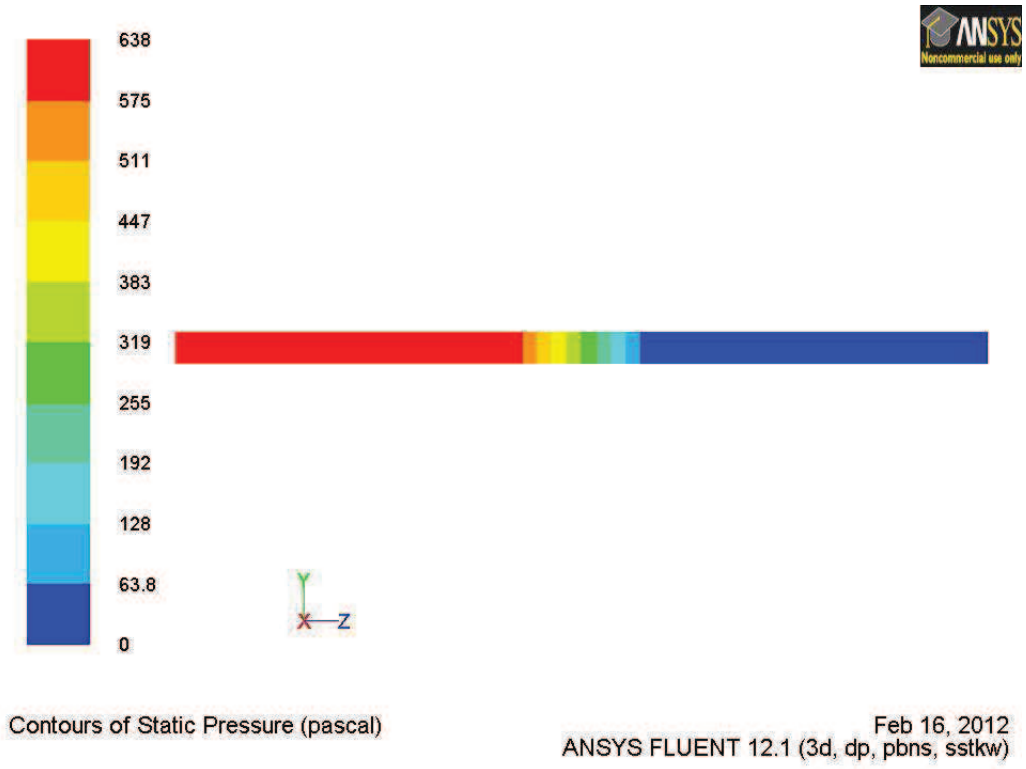

Figure 6: Static pressure, porous tube

These results were reached with very coarse mesh so it is still early to do some conclusions based on these results, first there is a need to prove that mesh and turbulent model are suitable for this case.

3.5 Mesh influence

Even though mesh in a single tube test (see Figure 2) have a very good skewness factor, it is still very coarse. The more cells the better mesh quality but also the

longer calculation time is. New mesh was created. Unlike the previous case the boundary layer was created on the inlet face attached to the wall with a usage of size function. This is because near wall region is characterized by large gradients. Then the rest of the inlet face were meshed with a very fine grid as it can be observed on Figure 7, where on right hand side there is also a mesh quality report with the green histogram which confirms very good mesh skewness factor since 62 % of all cells are in interval <0;0.1) and 26 % in interval <0.1;0.2). This geometry model of full-length U-tube and its mesh were created in Gambit®. Then task was transferred to Fluent®where the same parameters like for lower quality mesh were set (see Table 3). The calculation procedure was done on the cluster server.

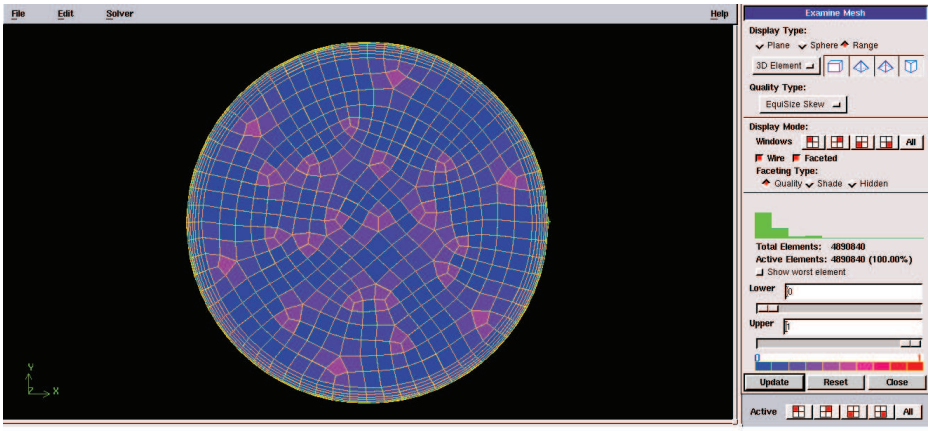

Figure 7: Fine mesh

3.5.1 Mesh influence results

The results from a fine meshed full-length U-tube were unexpected. Values of static pressure in comparison with coarse mesh from a single tube test were diametrically different (see Table 7). The total pressure drop of a fine meshed full-length U-tube differs about 38 %, we assumed the difference of 10 % maximum 20 % but not almost double one. Considering these results the decision to do more testing was made. Series of meshes were created. Started with original coarse mesh from a single tube test we made every following mesh finer. In the ended we end up with 6 cases, where last 2 included a boundary layer (see Figure 8). The number under the picture indicates the number of nodes on the inlet circle. The more nodes the finer mesh is. The similar parameters were set again and the

calculation was done. The results were written into Table 8.

Table 7: Static pressure in monitors, mesh influence

	U-pipe, rough mesh	U-pipe, fine mesh
inlet [Pa]	691.35	430
m1 [Pa]	668.41	410
p_start [Pa]	663.47	406
p_end [Pa]	23.34	14
m2 [Pa]	4.83	2.7
outlet [Pa]	0	0

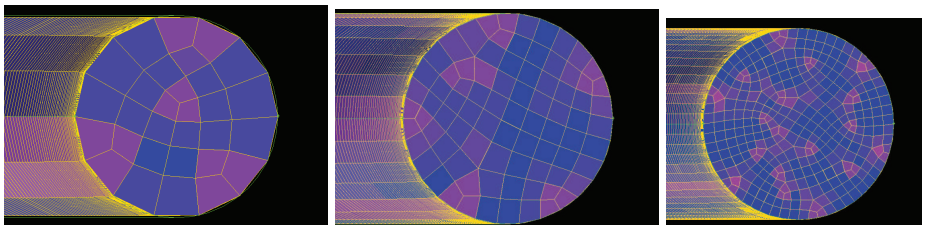

(a) 14 **(b)** 30 **(c)** 60

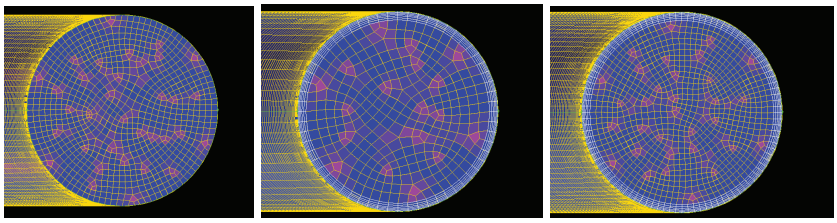

(d) 100 **(e)** 60+BL **(f)** 100+BL

Figure 8: Growing quality of mesh from a) to f)

To prove how fine mesh is Y+ value at the wall and the number of total elements were added into the table. This dimensionless wall number can be calculated by Eq. (11). Where ρ is density of the fluid, $v_\tau$is friction velocity, y is distance from the wall and μ is dynamic viscosity of the fluid.

$$Y+ = \frac{\rho v_\tau y}{\mu} \tag{11}$$

According to Fluent manual [4] we should avoid interval <5;30> because Y+ belongs to a buffer layer here. All of our tested meshes fulfilled this condition

however it is also written that for the near wall modeling approach should be Y+ around 1 and it is acceptable if Y+ < 4. Also there should be at least 10 cells in the viscosity-affected near-wall region (Re_y<200). Wall-distance-based turbulent Reynolds number Re_yserve to find demarcation of the two regions, viscosity-affected region and a fully-turbulent region. Re_y is determined by Eq. (12), where the meaning of constants is the same as in Eq. (11) and k is turbulent kinetic energy.

$$Re_y = \frac{\rho y \sqrt{k}}{\mu} \tag{12}$$

The data from all cases were taken and it was found out that viscous near-wall region thickness is δ=4.1 mm (see Figure 9). Only last two finest meshes with boundary layer satisfy all these conditions therefore results, which are almost identical for both mesh, should be declared as the right ones. But as you can observe in Table 8 or in Figure 10 values of total static pressure are decreasing and approaching the theoretical values calculated by Darcy-Weisbach equation (4) then we skip case d-100 since Y+ value indicate that we are in the middle of restricted zone but then there is a massive drop for last two cases which have very fine mesh with the boundary layer.

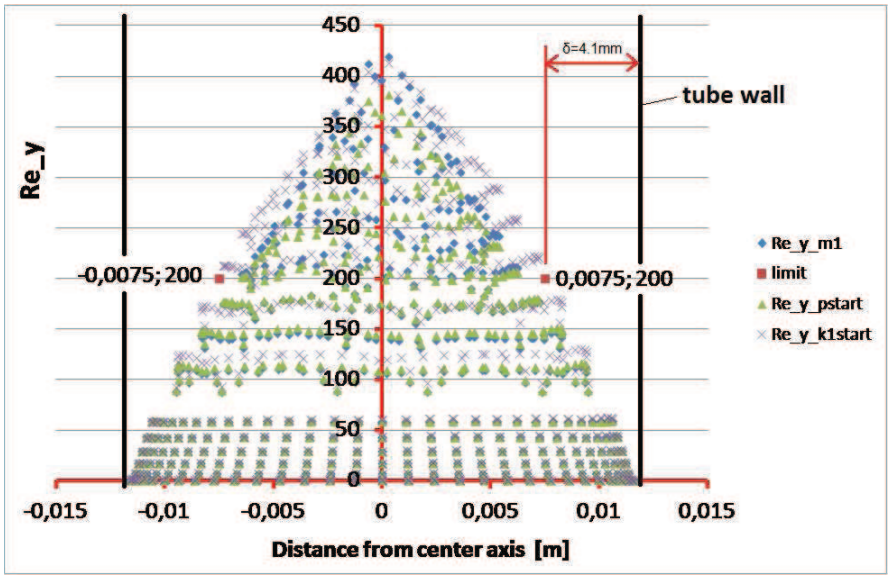

Figure 9

Table 8: Static pressure in monitors, using different mesh quality (see Figure 8)

	a-14	b-30	c-60	d-100	e-60+BL	f-100+BL	Theory
inlet [Pa]	691.35	657.08	627.86	600.08	426.40	425.32	609.40
m1 [Pa]	668.41	634.30	603.40	575.71	407.36	406.26	592.18
p_start [Pa]	663.47	629.45	598.82	571.43	404.18	403.09	587.88
p_end [Pa]	23.34	24.20	22.72	21.66	15.37	15.38	21.52
m2 [Pa]	4.83	4.44	4.17	3.99	2.86	2.86	4.30
outlet [Pa]	0	0	0	0	0	0	0
Y+ wall	90.37	50.22	25.19	14.95	1.77	1.78	
Number of elements	20 580	57 154	226 380	611 912	475 398	1 039 290	

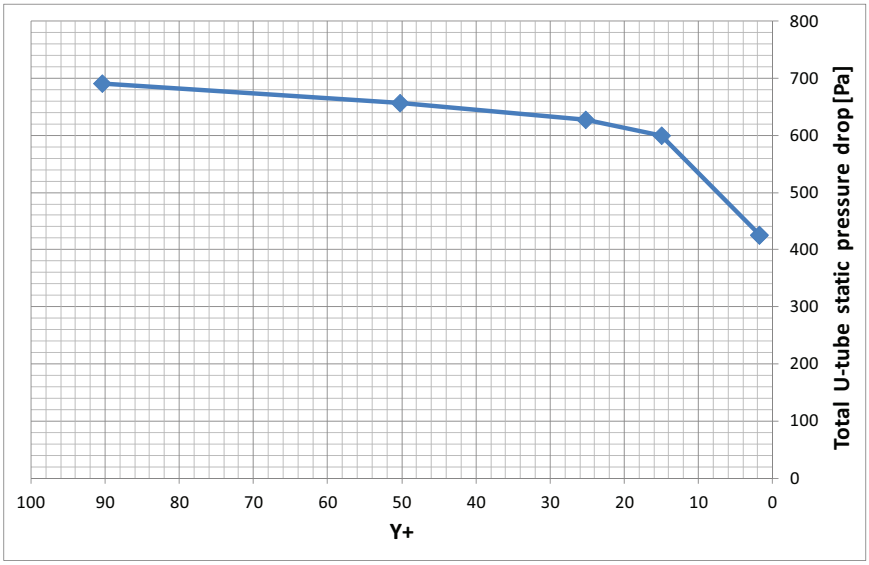

Figure 10: Pressure drop in dependence on Y+

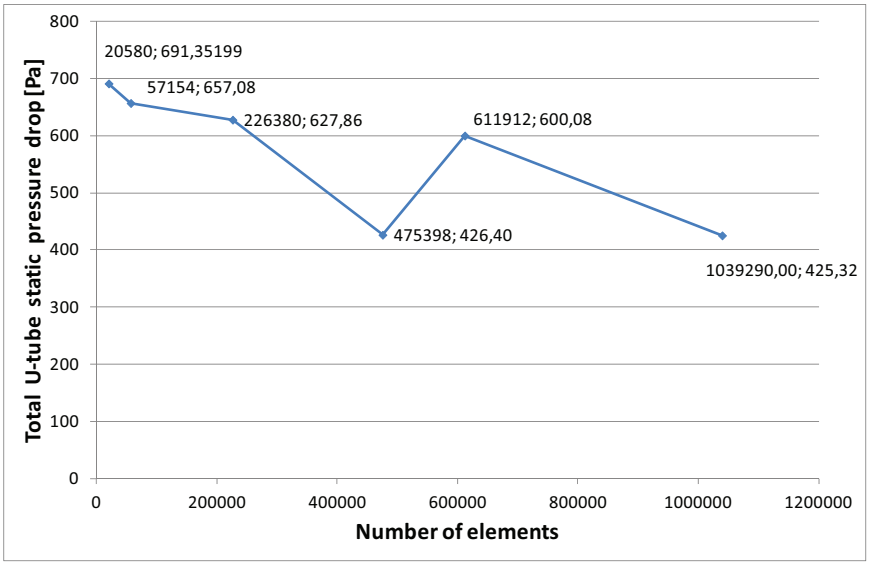

Figure 11: Pressure drop in dependence on number of elements

It turned out that these last two cases including boundary layers had the first adjacent cell to the wall of height 0.2 mm but roughness of wall was set to be 0.25 mm. According to Fluent manual [4] one should make sure that the distance from the wall to the centroid of the wall-adjacent cell is greater than wall roughness. This explained those strange values calculated with the finest meshes. Then a lot of attempts to create suitable mesh were done. But it turned out that it is impossible to create mesh with Y+ in range of 1 with wall adjacent cell higher than 0.5 mm. So a different strategy was chosen. Instead of SST k-ω turbulence model which uses near-wall modeling approach and requires very fine mesh near the wall, it was switched to k-ε realizable turbulence model with standart wall functions. For wall functions approach is written that value of Y+ should be in interval <30;300> and it is recommended to stay close to a lower value. This was easily achieved with mesh which has 40 nodes on inlet face. Then Y+ value for this case is 35. New calculations were done (see Table 9). As can be noticed the values are in better agreement than before and even closer to the theory. There is now only 4% difference in pressure drop between U-tube and porous tube.

This section proved that we need to be very careful with the selection of the proper turbulence model and suitable mesh and that there are lot of factors which need to be considered to achieve correct results.

Table 9: Results with k-ε realizable turbulent model

	U-tube, 40 nods on inlet face, k-ε	Porous tube, 40 nodes on inlet face, k-ε	Theory
inlet [Pa]	584.18	610.94	609.40
m1 [Pa]	562.61	588.42	592.18
p_start [Pa]	558.17	583.43	587.88
p_end [Pa]	21.35	25.96	21.52
m2 [Pa]	3.92	4.08	4.30
outlet [Pa]	0	0	0
Y+ wall	35.60	38.00, (35.72 for porous section)	
Number of elements	104 958	50 337	

3.6 Temperature influence

Due to a porous zone application we are now able to simulate the fluid flow in a heat-exchanger in a fair amount of time. But since the heat-exchanger´s main function is an exchange of the heat, then there is a need to consider heat transfer. First we turn on energy equation and introduce the heat source. In previous chapters the temperature and all fluid properties were constant. Now the temperature will change and with it also fluid properties, which will cause raise of pressure drop. Then we will try to implement this additional pressure drop caused by the temperature into the porous zone and let the energy equation turn off. This will save computational time.

3.6.1 Calculations and settings

According to the measured data from the heat-exchanger the inlet temperature is 70 °C and it warms up to 340 °C at the outlet. There are available also fluid properties data which can be seen in Table 10. Since we have only inlet and outlet data we assume these fluid properties to have a linear dependency on the temperature. According to the measured data process waste gas which flows through HX is quite close with the composition to air and air properties obey a linear dependency on the temperature (or it can be approximated as linear in

the certain temperature range). This was confirmed from several sources [9, 10] and also proved by calculations. The density ρ can be calculated by Eq. (13), which is the version of the ideal gas law, where p_a is atmospheric pressure, M is molar weight, R is universal gas constant and T is thermodynamic temperature. Viscosity μ of air can be determined by empirical Eq. (14), where μ_0 is dynamic viscosity at temperature t = 0°C, μ_0= 1.71x10^{-5}Pa-s and t is temperature in °C.

$$\rho = \frac{p_a \cdot M}{R \cdot T} \tag{13}$$

$$\mu = \mu_0 + 0.04747 \cdot t - 0.00002 \cdot t^2 \tag{14}$$

Conservation of energy for the steady state flow of a fluid in a tube can be written as Eq (15), where $\dot{m}$ is a constant mass flow rate, c_p is specific heat, T_e is temperature at the outlet and T_i at the inlet [11].

$$\dot{Q} = \dot{m} \cdot c_p (T_e - T_i) \tag{15}$$

Software Fluent provides a lot of possibilities to introduce energy to a boundary condition. Options are constant heat flux on the surface, constant temperature on the surface, convection and radiation. The most suitable for this case seems to be constant heat flux on the surface, because radiation is neglected and it is very difficult to determine a convection heat transfer coefficient. The constant temperature on the surface is also a good approach but just not so suitable for this case. The total heat flux calculated by Eq. (15) was divided by the surface of the single full length tube and then by the surface of the porous tube. These calculated values were set in Fluent and also wall thickness was added. Then the calculation was started.

$$\dot{Q} = 1406.5 \ W$$

$$A_{U-tube} = 0.516 \ m^2$$

$$\dot{q}_{surf,U-tube} = \frac{\dot{Q}}{A_{U-tube}} = 2725 \ W/m^2$$

Table 10: Measured fluid properties at inlet and outlet

	Inlet	Outlet
Temperature [°C]	70	340
Density [kg/m^3]	0.992	0.534
Heat capacity [kJ/kg-K]	1.22	1.289
Thermal conductivity [W/m-K]	0.0269	0.046
Viscosity [Pa-s]	0.0162	0.0267

3.6.2 Geometry

Most suitable mesh and turbulence model were found in the previous section. Therefore there were used exactly the same meshes and settings like before. The only change was that energy equation was turned on and heat flux on a surface was implemented.

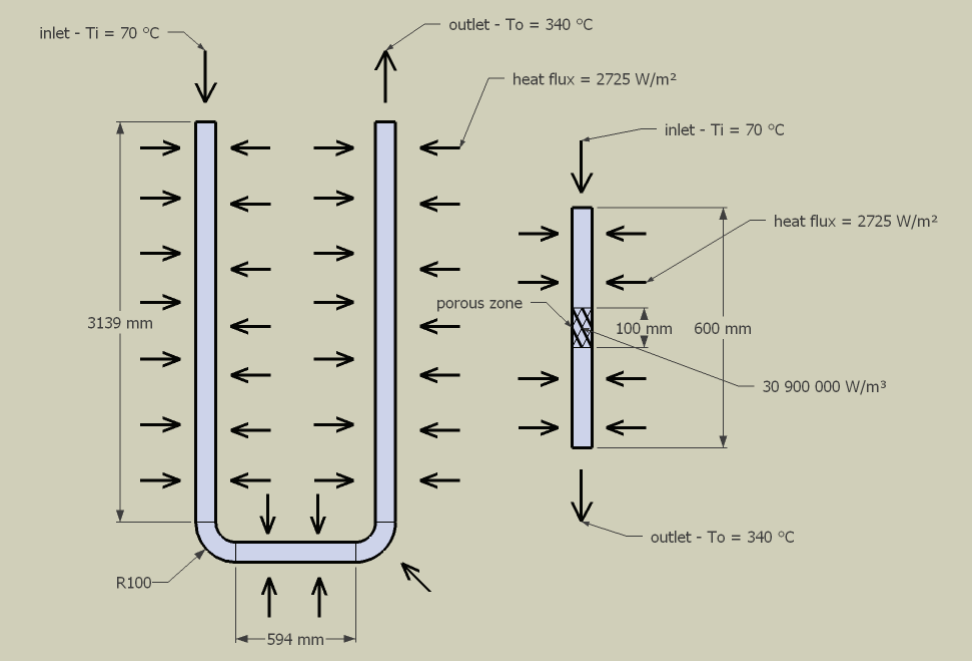

Figure 12: Scheme of heat transfer

3.6.3 Results

All fluid properties (except density, which follows ideal gas law) were defined to obey the linear dependence on the temperature. The results are not a big surprise. Because of the rising temperature gas will expand and the density will be dropping. This has an effect on the velocity of a fluid, which is rising and with rising velocity, pressure drop is also rising. This can be seen in Table 11.

Table 11: Fluid properties and pressure drop dependence on temperature for U-tube

Monitor name	Distance of monitor from inlet [m]	Temp. [°C]	Density [kg/m^3]	Velocity [m/s]	Static pressure [Pa]
inlet	0	70	1.04	9,99	840.14
m1	0.2	79	1.02	10,20	817.19
p_start	0.25	81	1.01	10,25	812.31
p_end	7.05	328	0.58	17,27	38.67
m2	7.25	336	0.57	17,47	7.13
outlet	7.3	337	0.57	17,52	0

The porous tube is much shorter than the full-length U-tube. This mean that surface heat flux is much higher and in the simulation the wall temperature increased over 1000 °C. Although the area-weight average outlet temperature was as desired, it was clear from the visualization that this very high wall temperature influences fluid properties close to the wall, which is undesired. It was calculated that the porous zone represents 93 % of the length of a full length U-tube. So logically in the porous zone there should be generated 93 % of the total heat income. Therefore the total heat flux was multiplied by 0.93 and then divided by the volume of the porous zone and it was implemented as a volumetric energy source term (see Figure 13). This solution ensures that the start and the end of the porous tube where is not the porous zone has the same heat flux as in the case of U-tube. With this solution we avoided wall overheating. Results can be observed in Table 12.

$$A_{porous} = 0.044 \ m^2$$

$$\dot{q}_{surf,porous} = \frac{\dot{Q}}{A_{porous}} = 32160 \ W/m^2$$

$$r = \frac{L_{porous}}{L_{U-tube}} = \frac{6.581}{7.081} = 0.929$$

$$\dot{Q}_{porous} = \dot{Q} \cdot r = 1307 \ W$$

$$V_{porous} = 4.227 \cdot 10^{-3} \ m^3$$

$$V_{source,porous} = \frac{Q_{porous}}{V_{porous}} = 3.09 \cdot 10^7 \ W/m^3$$

$$Q_{porous,start+end} = Q - Q_{porous} = 99.318 \ W$$

$$A_{porous,start+end} = 0.036 \ m^2$$

$$q_{surf,porous,start+end} = \frac{Q_{porous,start+end}}{A_{porous,start+end}} = 2725 \ W/m^2$$

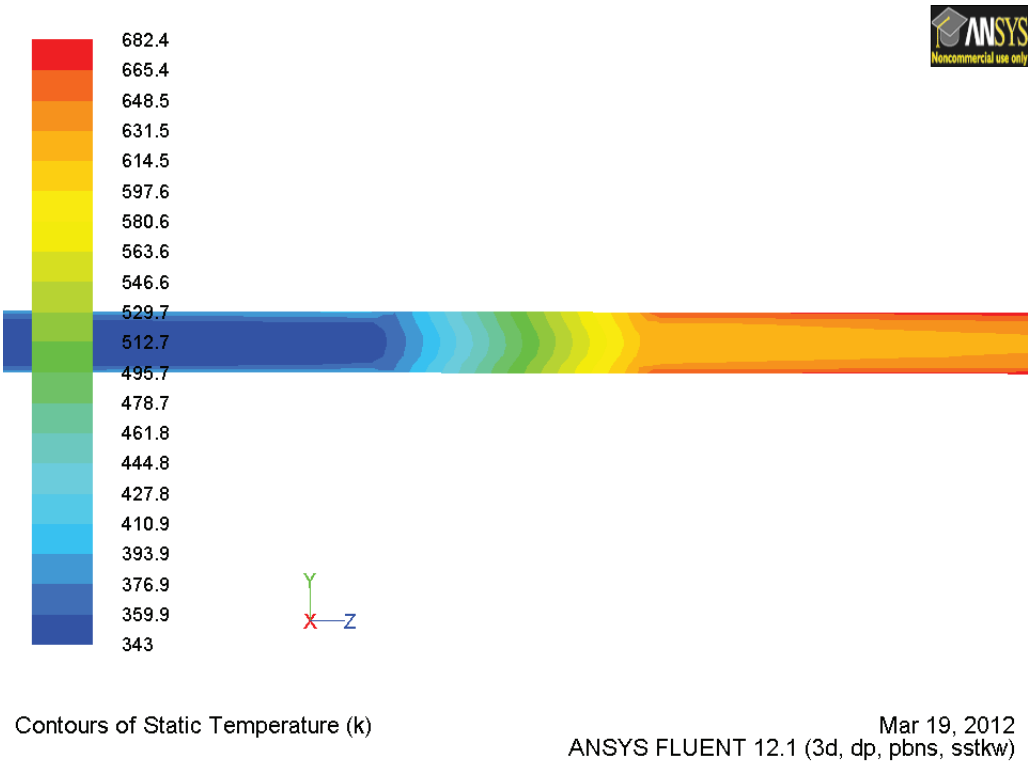

Figure 13: Porous tube with volumetric energy source term

Table 12: Fluid properties and pressure drop dependence on temperature for porous tube

Monitor name	Distance of monitor from inlet [m]	Temp. [°C]	Density [kg/m^3]	Velocity [m/s]	Static pressure [Pa]
inlet	0	70	1.04	9.77	889.10
m1	0.2	78	1.01	9.99	865.27
p_start	0.25	81	1.00	10.01	859.78
p_end	7.05	322	0.59	17.01	46.38
m2	7.25	332	0.58	17.32	7.44
outlet	7.3	334	0.58	17.37	0

3.6.4 Other temperature solution

To be able to examine the temperature influence on the pressure drop it was necessary to turn on the energy equation and implement the heat flux, this mean more computational cost. The aim of this thesis is to cut down the computational cost but at the same time to achieve correct results. It is standart procedure to do HX calculations with bulk mean fluid temperature Eq. (16) [11, 12].

$$T_b = \frac{T_i + T_e}{2} \tag{16}$$

Where $T_e$is temperature at the outlet and $T_i$at the inlet. Therefore a new calculation was done with the constant bulk temperature T_b. Using this solution there is no need to turn on energy equation and we were able to reduce the computational cost. But since energy equation is turned off then there is no possibility to set the inlet temperature. So fluid temperature is represented by fluid properties. As it was proved before with a reasonable accuracy we assume a linear dependency on the temperature. Therefore fluid properties (density and viscosity) were easily evaluated at T_b. The results are written into Table 13 together with the results from the previous cases, where the temperature was rising, for a comparison. It can be observed that there is approximately 10% difference between U-tube with the change of the temperature and U-tube with the constant bulk temperature T_b, which is acceptable but as was noticed before the simulation with the porous zone has always a little bit bigger pressure loss than the full length U-tube so in this case there is only 6% difference between the U-tube with the change of the temperature and the porous tube with the constant bulk temperature T_b. This is an almost ideal case for us because with the reasonable accuracy we are able to replace the full length U-tube by a tube with the porous zone and neglect the heat transfer simulation.

Table 13: Comparison of heat transfer solutions

Monitor name	Static pressure in U-tube with constant T_b [Pa]	Static pressure in porous tube with constant T_b [Pa]	Static pressure in U-tube with change of temp. [Pa]	Static pressure in porous tube with change of temp. [Pa]
inlet	754.40	794.53	840.14	889.10
m1	726.72	765.67	817.19	865.27
p_start	720.95	759.18	812.31	859.78
p_end	27.60	33.47	38.67	46.38
m2	5.07	5.30	7.13	7.44
outlet	0	0	0	0

It is true that it is the standart procedure to do HX calculations with the bulk mean fluid temperature T_b. However this approach is suitable for theoretical calculations but not for CFD calculations where we want to consider flow not only in a tube section but also in diffuser and collector. Because flow properties would be influenced also in this sections and that is not desired. Solution is to implement additional pressure drop caused by the temperature straight into the porous zone via inertial resistance coefficient C_2. The inertial resistance coefficient C_2 is dependent on D'Arcy-Weisbach friction coefficient λ, the length of tube which is going to be replaced by porous zone L_{total}, hydraulic diameter D and the length of porous zone L_{porous}. This mean that it is independent on fluid properties and that it is possible to adjust C_2 only through L_{total}. Therefore there was calculated pressure drop Δp_1 with fluid properties at 70 °C and pressure drop Δp_2 with fluid properties at the bulk mean fluid temperature. Then was calculated their difference Δp_{temp} which is additional pressure drop by the temperature rise. D'Arcy-Weisbach equation was reformulated and there was calculated $L_{temp,img}$ which is imaginary length of the tube representing Δp_{temp}. $L_{temp,img}$ was added to the length of tube which is going to be replaced by the porous zone and then new C_2 was calculated.

$$\Delta p_1 = \lambda \cdot \rho_1 \frac{L \cdot v_1^2}{D \cdot 2} = 603 \ Pa$$

$$\Delta p_2 = \lambda \cdot \rho_2 \frac{L \cdot v_2^2}{D \cdot 2} = 815 \ Pa$$

$$\Delta p_{temp} = \Delta p_2 - \Delta p_1 = 212 \ Pa$$

$$L_{temp,img} = \frac{\Delta p_{temp} \cdot D \cdot 2}{\lambda \cdot \rho_2 \cdot v_2} = 1.825 \ m$$

$$L_{total} = L + L_{temp,img} = 8.333 \ m$$

$$C_2 = \frac{\lambda \cdot L_{total}}{D \cdot L_{porous}} = 139.4$$

The previous geometry model and mesh was used to test this approach. The results can be observed in Table 14. Other approaches are added into table for a quick comparison. It can be noticed that this solution is the furthest from U-tube with the constant heat flux on the surface which is considered to be the reference state. But the deviation is 7-11 % and that is still acceptable in engineering calculations.

Table 14: Comparison of heat transfer solutions

Monitor name	Static pressure in porous tube with temperature influence include in C_2 [Pa]	Static pressure in porous tube with constant T_b [Pa]	Static pressure in porous tube with change of temp. [Pa]	Static pressure in U-tube with change of temp. [Pa]
inlet	781.16	794.53	889.10	840.14
m1	753.44	765.67	865.27	817.19
p_start	720.95	759.18	859.78	812.31
p_end	26.22	33.47	46.38	38.67
m2	4.06	5.30	7.44	7.13
outlet	0	0	0	0

3.7 Summary

In this chapter we provided a guideline how to decrease number of elements when dealing with CFD modeling of large HX. The main point is to straighten all tubes and then replace a major part of it with the porous zone which will have almost the same pressure drop and the heat income as the length it represents. The pressure drop difference between the full length U-tube and the porous tube is 4 %. It needs to be remembered that mesh has a big influence on the result and therefore it must be done properly and according to the turbulence model specification. As the best choice for our case appeared to be k-ε realizable turbulence model with standart wall functions, hexahedral mesh with 40 nodes on the inlet face and Y+ value of 35. Also it is important to check if local loss coefficients for bendings are suitable if we want to straighten the tubes and make the task simpler. When we introduce heat then the most suitable model is constant heat flux on the surface although in the porous zone there is a need to use volumetric heat source due to overheating of the wall and influencing flow properties. However this solution requires to turn on energy equation. To avoid this addition of the computational cost there is a possibility to make a calculation with bulk mean fluid temperature or to implement additional pressure drop caused by the temperature straight into the porous zone via inertial resistance coefficient C_2. The last approach is the most effective and difference between complex modeling of the heat transfer and adding the heat transfer effects into porous zone is 7 %.

4 Real heat exchanger application

There was a task to identify why some of heat-exchanger (HX) tubes are being chocked up. The chocking effect is often caused by a nonuniform distribution and vorticity of the flow. To be able to confirm this hypothesis the simulation with a usage of computational fluid dynamics (CFD) needs to be done. HX consists of a main pipe with the diameter 0.58 m, which is bended by 90°. Through this main pipe process waste gas (PWG) flows to diffuser and then is distributed to 1113 tubes, which are U-shaped, thus they have various total length from 7 m to 9.1 m. There are 17 rows of tubes and in each row there are 64 or 65 tubes (staggered tube arrangement) of the same length. For a better visualization look at the scheme of HX in Figure 14. The inner diameter of pipes is 0.0232 m and thickness of the wall is 0.002 m. An estimated roughness height of the inner wall is 0.00025 m. In these 1113 pipes PWG is heated up and leaves HX through identical geometry as at the inlet. To HX inlets PWG with parameters listed in Table 15.

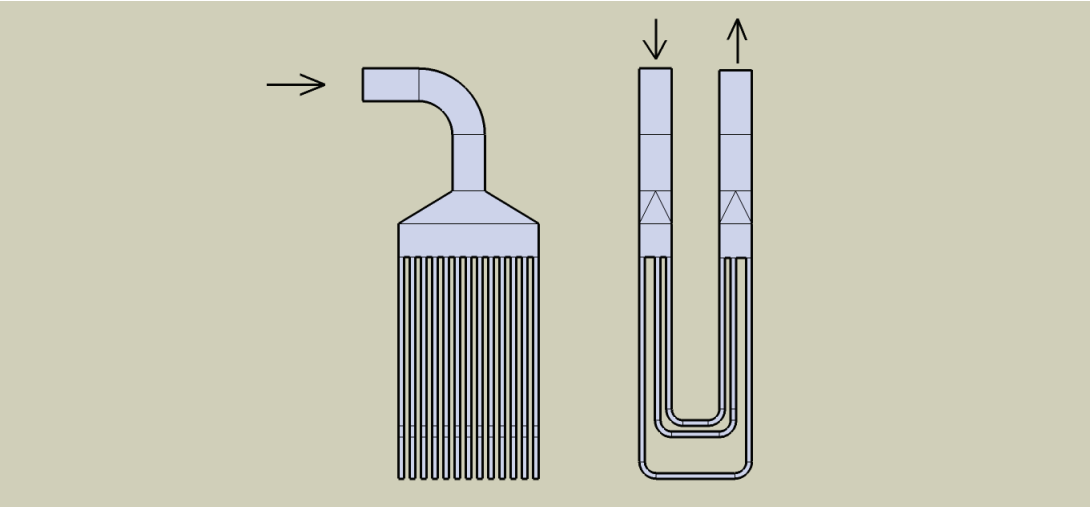

Figure 14: Scheme of HX

Table 15: Properties of inlet PWG

Mass flow rate	4.75 kg/s
Density	0.992 kg/m^3
Viscosity	1.62e-05 kg/m-s
Temperature	70.2 °C
Heat capacity	1.22 kJ/kg-°C

4.1 Pre-calculation processes

At first dimension data were gained from drawings. Then software Solid Works® was used to create a geometry model (Figure 15). The geometry model was transferred to software Gambit® where mesh was created with the help of my supervisor Ing. Jiří Vondál. Number of the cells is 10 075 000. Then mesh was exported to the Fluent®,where properties of fluid and the boundary conditions were specified (see Table 15), the turbulence model was selected to be k-ε realizable with non-equilibrium wall functions. Solution methods were set for SIMPLEC with skewness correction equals to 1. The first order upwind discretization was used and then switched to the second order after convergence was reached with the first order. Than an inertial resistance coefficient C_2 for each row of tubes was calculated and set (see Table 16). The whole calculation process was transferred to the cluster server.

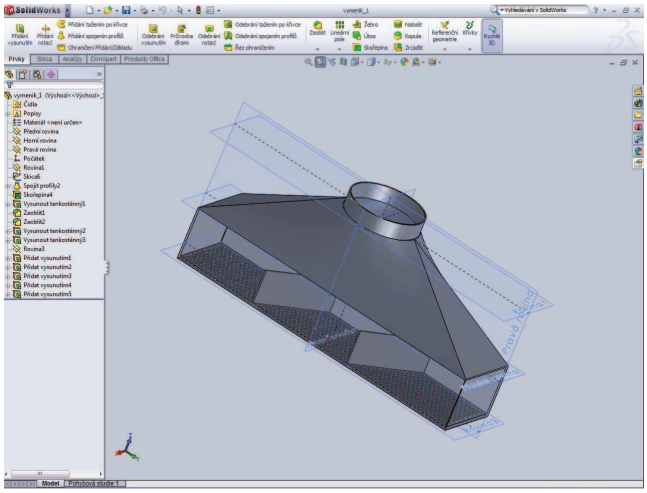

Figure 15: Geometry model of diffuser

Table 16: Lengths of pipes

Row number	Already straight sections [m]	Total length of straighten tube [m]	Length replaced by porous zone [m]	Inertial resistance coefficient C_2 [-]
1	6.874	7.008	6.508	106.598
2	7.000	7.134	6.634	108.669
3	7.127	7.261	6.761	110.740
4	7.253	7.387	6.887	112.810
5	7.379	7.513	7.013	114.881
6	7.506	7.640	7.140	116.952
7	7.632	7.766	7.266	119.023
8	7.759	7.893	7.393	121.094
9	7.885	8.019	7.519	123.165
10	8.012	8.146	7.646	125.236
11	8.138	8.272	7.772	127.307
12	8.264	8.398	7.898	129.378
13	8.391	8.525	8.025	131.449
14	8.517	8.651	8.151	133.520
15	8.644	8.778	8.278	135.591
16	8.770	8.904	8.404	137.662
17	8.897	9.031	8.531	139.733

4.1.1 HX results

The simulation on the cluster server converged successfully and results were obtained. Each of 1113 pipes had a monitor. The data describing the mass flow rate from each tube were collected and evaluated to see if there are any major differences in the distribution of the flow through tubes. Mass flow rate was averaged by rows in tubes with the same length (x-direction) and also in tubes with all lengths (x-direction), for better visualization see Figure 16 where are plotted tubes center. The simulation was done with k-ε realizable turbulence flow model and also with k-ω SST turbulence flow model. Then both models were compared.

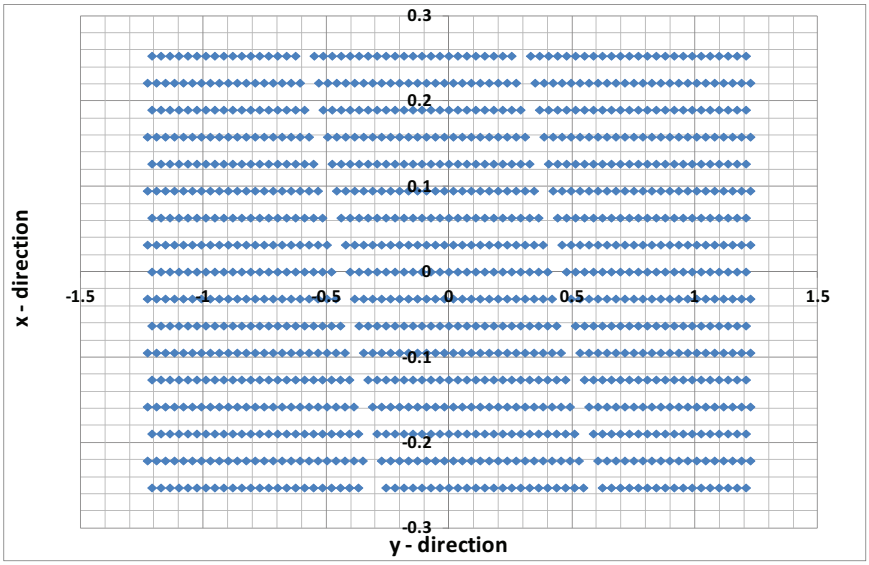

Figure 16: Tubes center

In Figure 17 it can be observed average mass flow rate trough tubes with the same length. There are 17 rows of tubes in x-direction with the same length. The highest average mass flow rate is in the row number 1, where tubes are the shortest and the lowest average mass flow rate is in the row number 17, where tubes are the longest. This phenomenon was expected because shorter tube means higher velocity, which cause higher mass flow rate. The mass flow rate average in rows changes very slightly and difference between the shortest row number 1 and the longest row 17 is only 10 %. This is because diffuser has in x-direction same width like a diameter of the main pipe, so the distributing effect in this dimension is low. However the line should be more linear then the one we plotted from gained data. It can be noticed that the k-ε realizable turbulence flow model and the k-ω SST turbulence flow model gave us almost identical results.

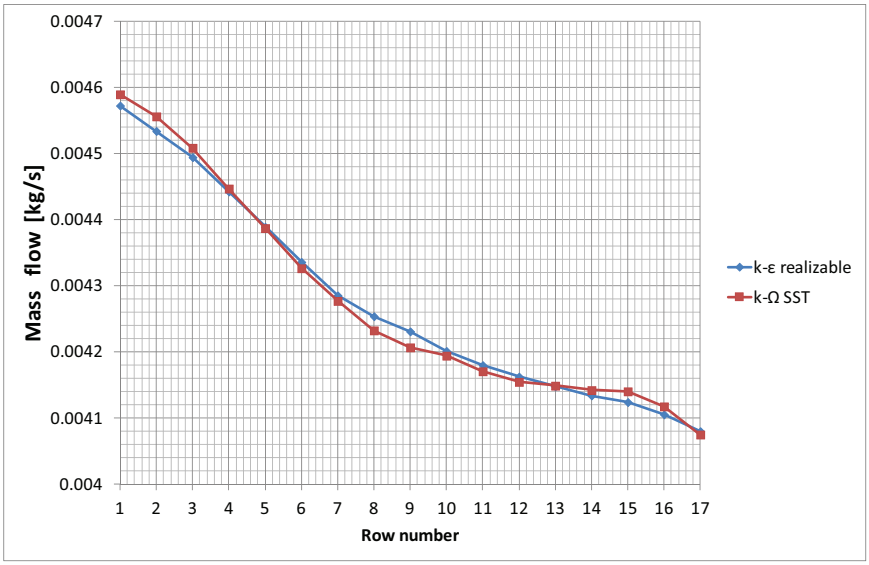

Figure 17: Average mass flow rates in 17 rows (x-direction)

Data was averaged by rows also in y-direction and in the Figure 18 can be observed that flow distribution by diffuser is really poor and that 2 partitions which are placed in diffuser causing vortexes. That can be nicely seen in Figure 18 where data named down_wall and up_wall are fluctuating a lot. Most of the flow is going through middle section and then section named down. The fact why flow is flowing more through section down then section up is caused by bending of the main pipe (see Figure 19). The difference between the highest and the lowest mass flow rate is 25 %. Every data-line match with its color with color of the spot in scheme under the graph. The average mass flow rate through left section named "down" is 0.00416 kg/s, through middle section with a same name it is 0.00455 kg/s and trough right section named "up" it is 0.00398 kg/s. The difference between average mass flow rates in middle section and right section is 12.5 %. And 8.6 % between middle section and left section.

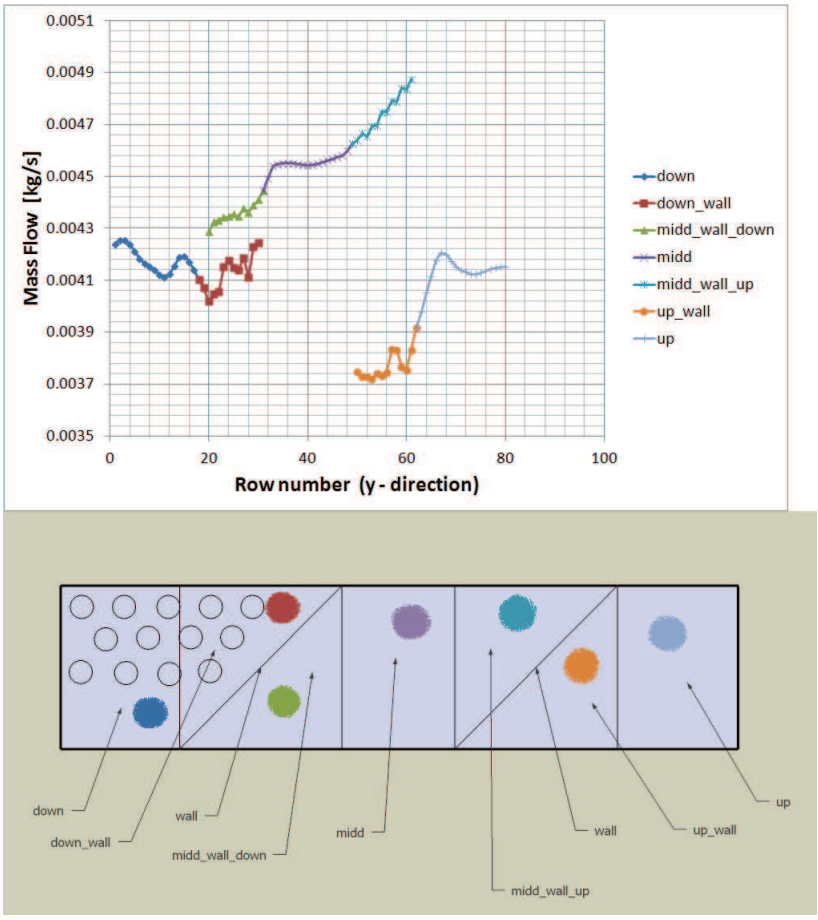

Figure 18: Average mass flow rates in 80 rows (y-direction)

Vortexes were confirmed and located by pathlines visualization on Figure 20 and contours of velocity magnitude, contours of turbulent intensity and contours of vorticity magnitude on Figure 21.

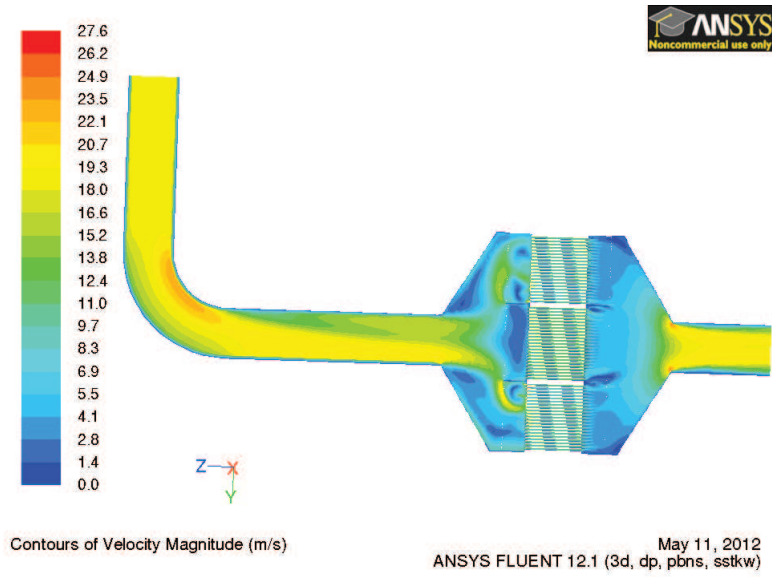

Figure 19: Bending effect of the main pipe

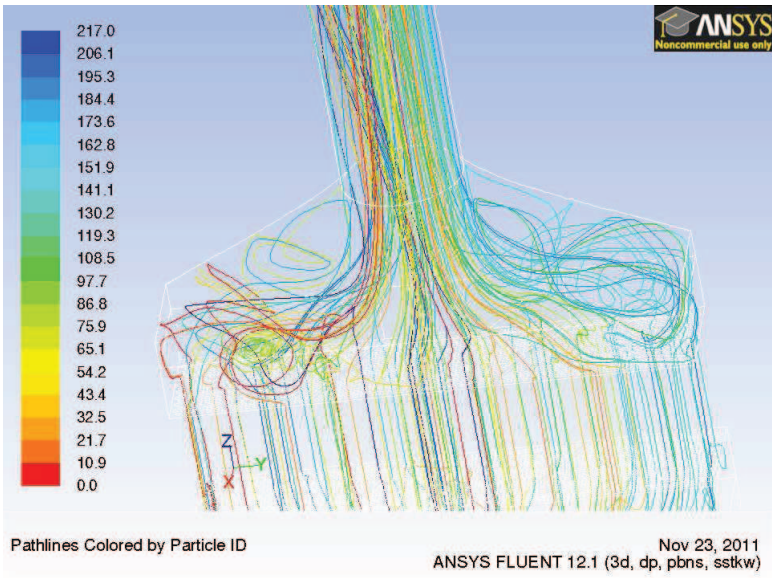

Figure 20: Pathlines visualization

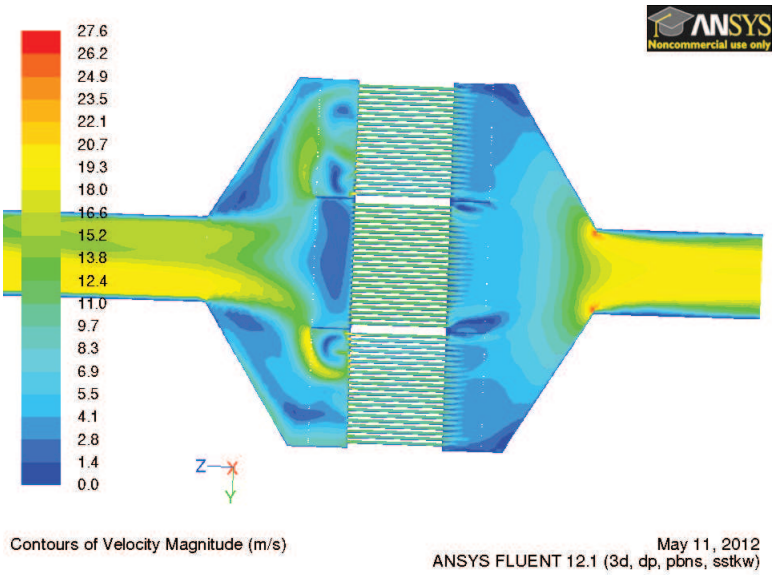

(a) contours of velocity magnitude

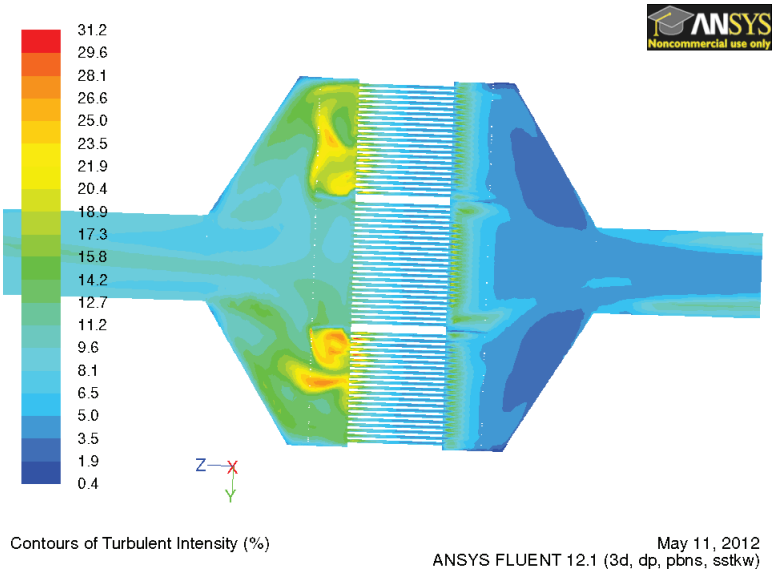

(b) contours of turbulent intensity

Figure 21: Visualize results

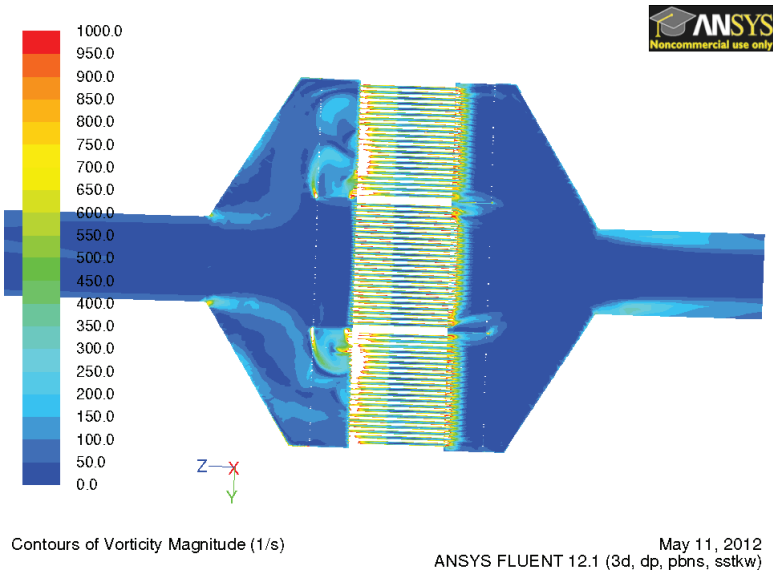

Figure 22: Visualize results, contours of vorticity magnitude

The Figure 23 shows the real heat exchanger. Notice that tubes inlets are choked in the same areas where we identified vortexes with CFD simulation. Therefore our simulation seems to be correct.

(a) **(b)**

Figure 23: Pictures from real HX

Based on these results we were able to identify problematic places. As the main reason of all problems were identified inefficient diffuser performance. Therefore the decision to change diffuser design was made.

4.2 Heat exchanger with new diffuser design

The solution with 2 rows of baffle and longer diffuser was chosen. Diffuser high was 592 mm and now it is 1663 mm. There are five guiders which are creating first row of baffle. The middle guider is the longest (1298 mm) and it has 2 more guiders on each side, which are shorter (546 mm) and bended by 17 and 30 degrees in a direction from the central z axis in order to maximally distribute the flow. The first row of baffle should suppress effect of the main pipe banding and distribute flow more equally. The second row of baffle is created by ten guiders. Five guiders are in the left section behind the partition from the central z axis and other five are in the right section behind the partition. All the guiders have same turning like a partition. Fist three from the center are 137 mm high and other two are higher by 23 mm and 48 mm. The second row of baffle is created to prevent formation of vortexes. New 3D model was created. In Figure 24 can be seen all improvements. All parameters and settings remained unchanged. The calculation was done again on the cluster server. This time only with k-ε realizable turbulence flow model.

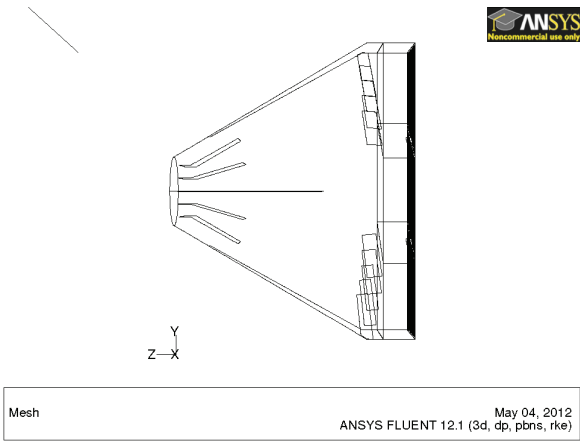

Figure 24: New diffuser design with 2 rows of baffles, Fluent

4.2.1 Results of heat exchanger with new diffuser design

Data from all monitors were taken and evaluated by rows in x and y direction (see Figure 16). In Figure 25 can be seen that averaged mass flow rates in rows with the same length (x-direction) has now more linear dependency, which is a good sign.

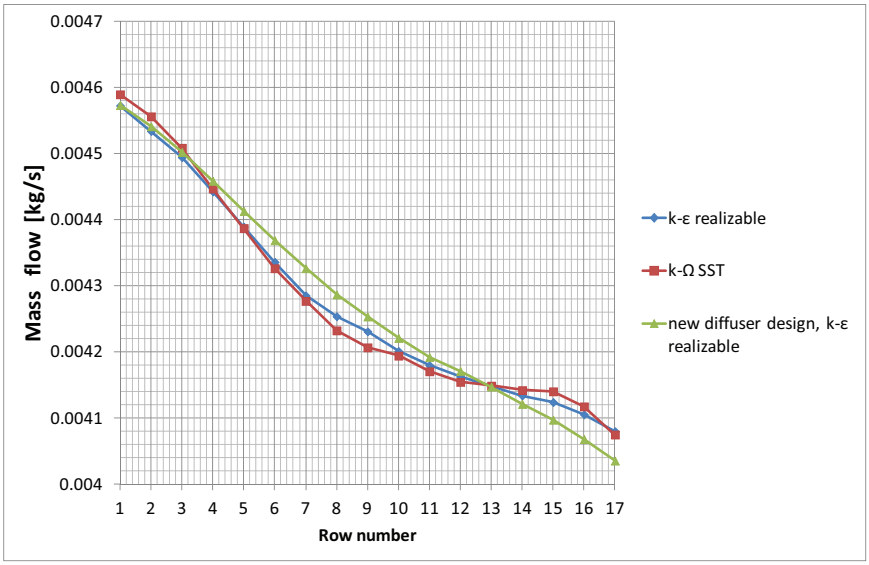

Figure 25: Comparison between mass flow rates of old and new diffuser design (x-direction)

Averaged mass flow rates in rows in y-direction can be observed in Figure 26. Notice that fluctuations in partitions areas are much smaller then with old diffuser design (grey colour) and also range of mass flow rate is not so wide. The difference between the highest and the lowest mass flow rate is 14 %, which is 11 % less then with the old design. The average mass flow rate through left section named “down” is 0.00441 kg/s, through middle section with a same name it is 0.00433 kg/s and trough right section named “up” it is 0.00414 kg/s. Notice that now the highest mass flow rate is going through left section. The difference between average mass flow rates in middle section and right section is now only 2 %. And only 4 % between middle section and left section. In the Figure 26 can be again seen effect of bending of main pipe. In this solution it is even higher due to the first row of baffle. This can be nicely observed in Figure 27.Effect of the new design can be also observed on Figure 28. There are no more vortexes and flow field is more uniform. The new design in not ideal and first row of baffle could be redesigned but it is improvement in comparison to old design.

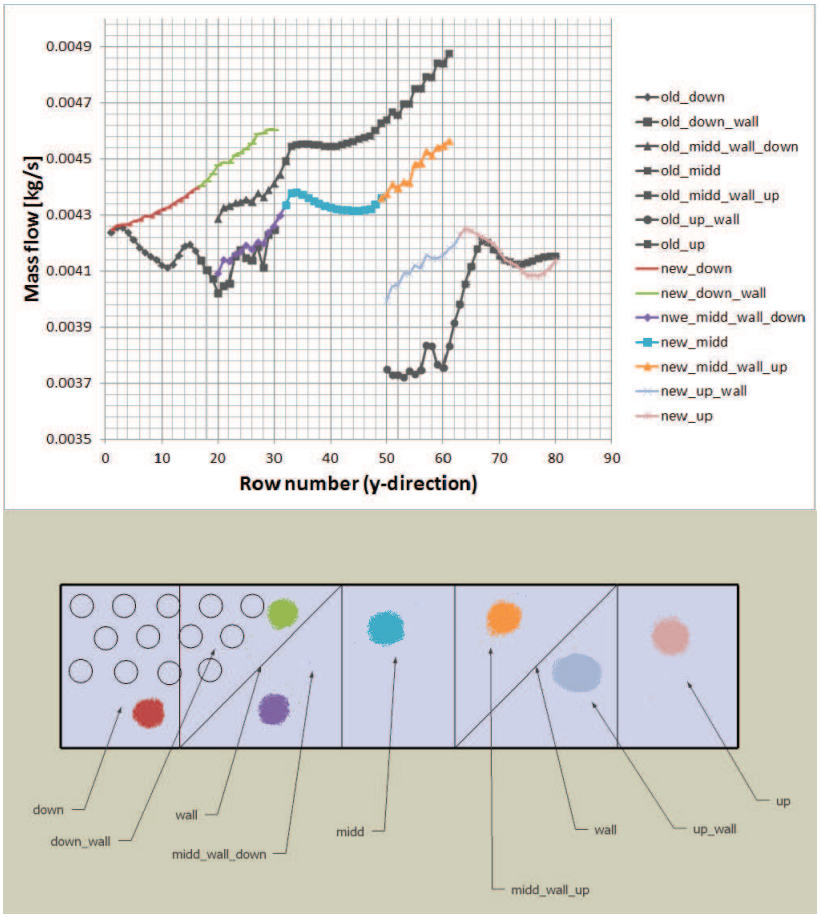

Figure 26: Comparison between mass flow rates of old and new diffuser design (y-direction)

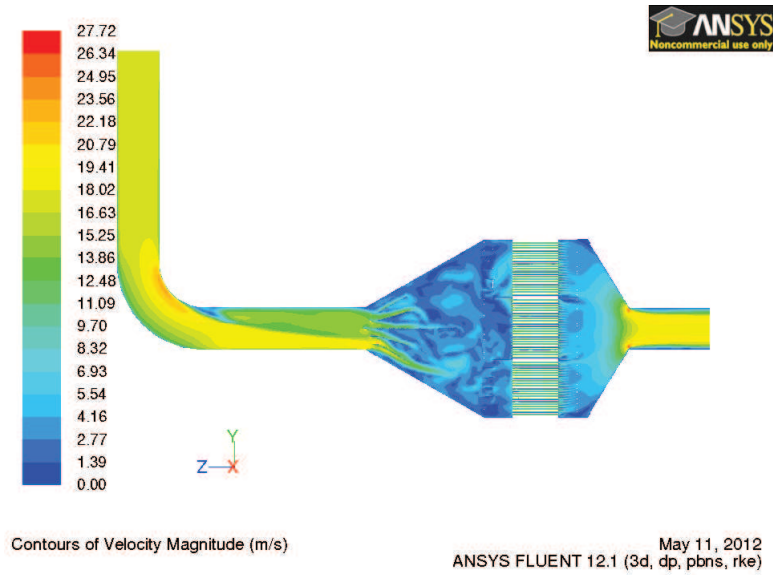

Figure 27: Visualize results with new diffuser design, Enhanced bending effect of the main pipe

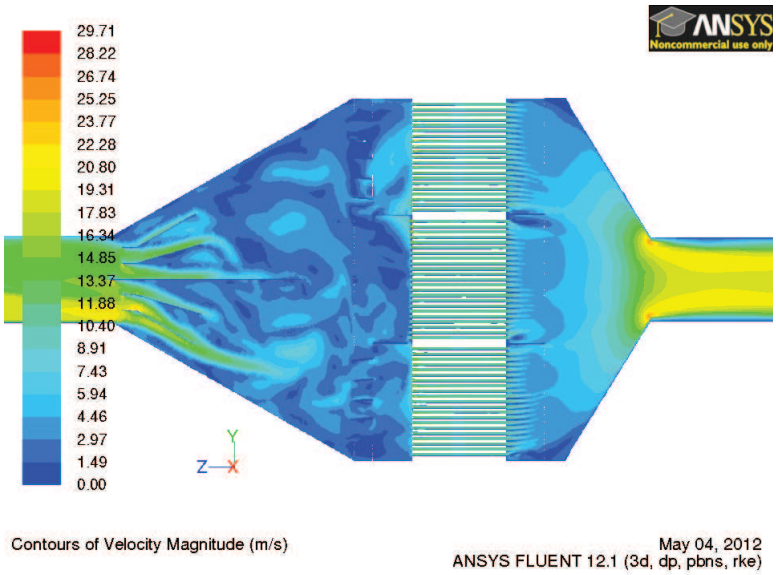

Figure 28: Visualize results with new diffuser design, contours of velocity magnitude

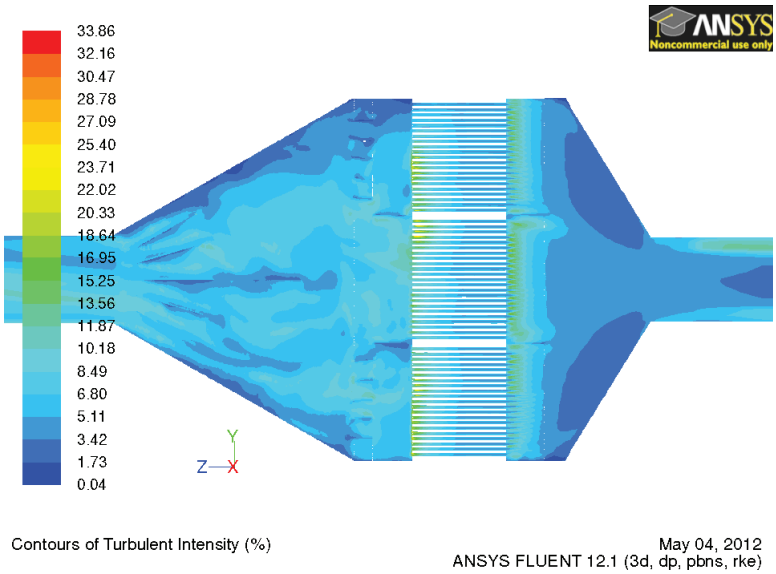

Figure 29: Visualize results with new diffuser design, contours of turbulent intensity

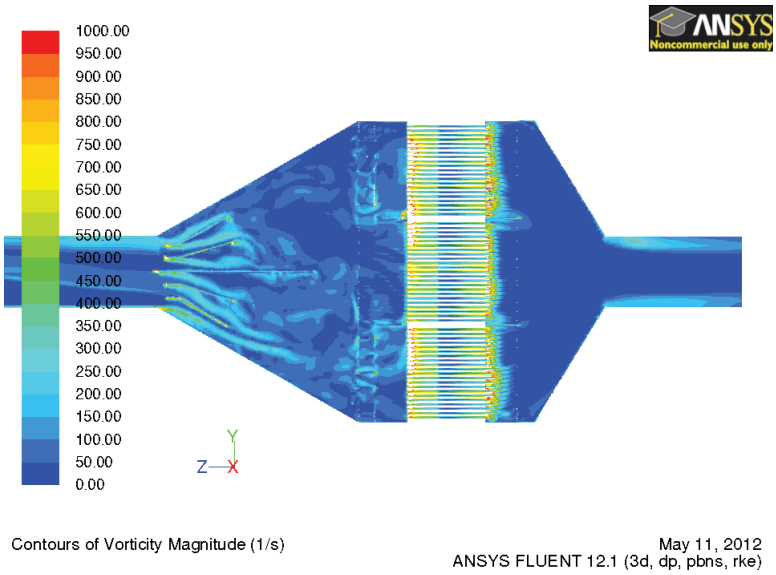

Figure 30: Visualize results with new diffuser design, contours of vorticity magnitude

4.3 Heat exchanger with new diffuser design and temperature influence

In a previous section there was examined the flow through HX but with the constant temperature. In this section we will implement the knowledge from the section 3.6 and simulate the influence of the temperature on the pressure drop. In section 3.6 were suggested 3 approaches. The first approach is to introduce surface heat flux on the parts without the porous zone and the volumetric heat source into the porous zone. This solution requires to turn on energy equation and due to it the computational cost is higher. The second approach is to let the energy equation turned off and make the calculation with fluid properties at a bulk mean fluid temperature, which is arithmetic average of the temperatures at the inlet and the outlet Eq. (16). But in this task the boundary condition for inlet is defined at the face of main pipe, therefor it is not possible to use this approach. Because that would mean that flow is influenced by the temperature also in diffuser section and that is not true. This situation calls for the third approach and that is to implement additional pressure drop caused by the temperature straight into the porous zone via inertial resistance coefficient C_2.

Detail procedure is described in section 3.6.4. New coefficients for each of 17 rows were calculated (Table 17) and then changed in calculation settings. All other parameters remained unchanged again.

Table 17: New C_2 coefficients including temperature difference

Number of the row	Total length of straighten pipe [m]	Length replaced by porous zone [m]	Imaginary additional length representing temperature influence [m]	Inertial resistance coefficient C_2 [-]
1	7.008	6.508	1.825	139.445
2	7.134	6.634	1.858	142.124
3	7.261	6.761	1.89	144.803
4	7.387	6.887	1.923	147.482
5	7.513	7.013	1.956	150.161
6	7.640	7.140	1.99	152.84
7	7.766	7.266	2.023	155.519
8	7.893	7.393	2.056	158.198
9	8.019	7.519	2.089	160.877
10	8.146	7.646	2.122	163.556
11	8.272	7.772	2.155	166.235
12	8.398	7.898	2.188	168.914
13	8.525	8.025	2.221	171.593
14	8.651	8.151	2.254	174.272
15	8.778	8.278	2.287	176.951
16	8.904	8.404	2.32	179.63
17	9.031	8.531	2.353	182.309

4.3.1 Results of heat exchanger with new diffuser design and temperature influence

Data were processed and compared with previous cases (see Figure 31). As can be noticed results are almost identical with previous case without temperature influence. This is caused by fact that inertial resistance coefficient $C_2$was increased in every row linearly. Because assumption was that each row has same inlet and outlet temperature. However this is certain only for the inlet temperature and very unlikely for the outlet temperature due to fact that tubes have different length. We will try to make some more precise assumptions in the next chapter.

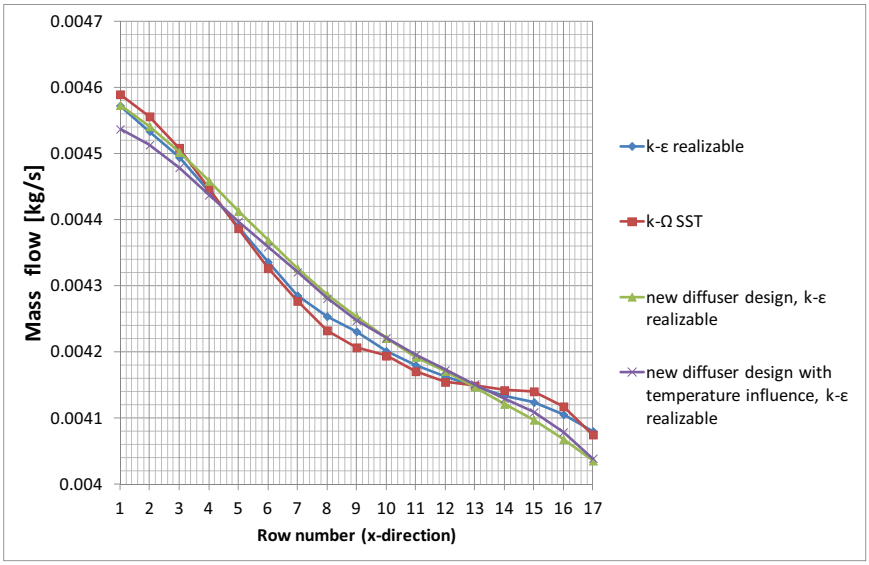

Figure 31: Comparison of mass flow rates in x-direction of old design, new design and new design with temperature influence

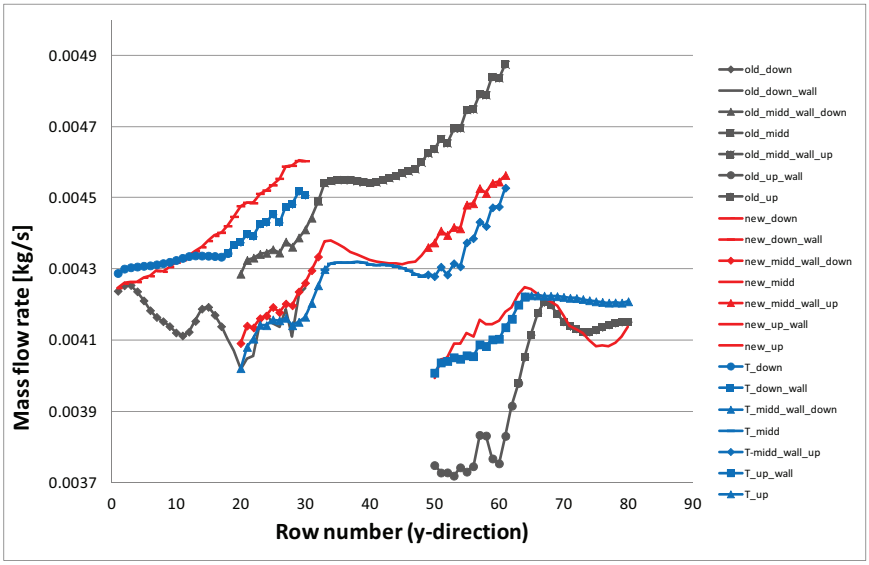

Figure 32: Comparison of mass flow rates in y-direction of old design, new design and new design with temperature influence

4.4 More precise inertial resistance coefficients for temperature influence

From measured data we know that the temperature at the outlet is 340 C but the temperature is measured after the collector. Because of different lengths of rows is outlet temperatures of rows also different. So measured temperature is basically the average of outlet temperatures from all rows. There are 2 main factors which are influencing heat transfer and changes with length of the tube. The first factor is area of tube. Longer tube means larger heat transfer area so higher heat transfer. The second factor is inner heat transfer coefficient. Longer tube means lower flow velocity, which has high influence on heat transfer coefficient. It is obvious that these 2 factors are clashing against each other. Therefore to be able to say which factor is more conclusive we need to do some calculations.

Consider there are 2 tubes with same inner and outer diameter. Tube number 1 is 1 m long and tube number 2 is longer by 10 % so it is 1.1 m long (see Figure 33). It can be proved by simple calculation that heat transfer area of tube number 2 is also larger by 10 % then heat transfer area of tube number 1.

$$A = \pi \cdot D_o \cdot L$$

$$\frac{A_2}{A_1} = 1.1$$

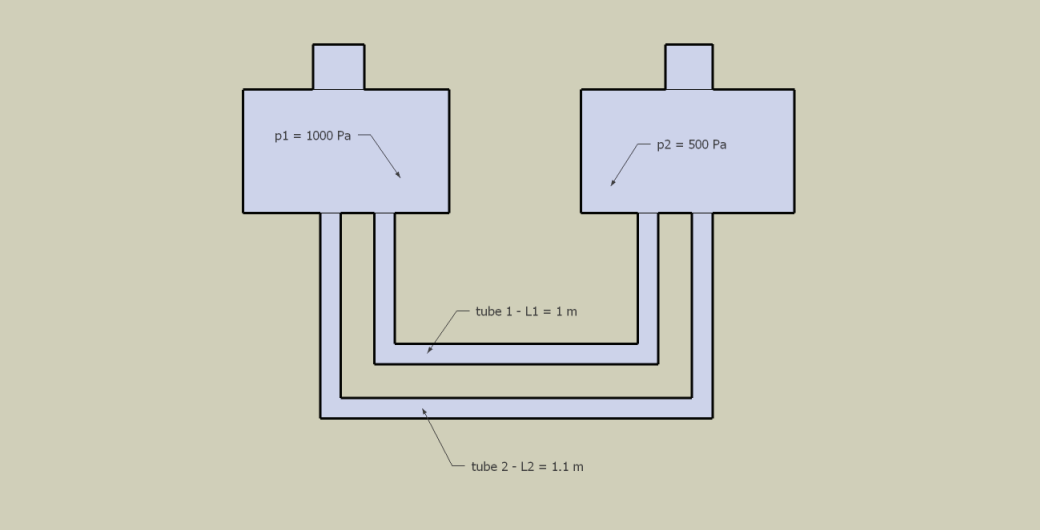

Figure 33: Scheme of tubes for more precise temperature influence

Then assume that both tubes are connecting diffuser where is pressure p_1=1000 Pa and collector where is pressure p_2=500 Pa. Therefore in each tube is pressure loss dp=500 Pa (see Figure 33). We are able to calculate velocities by using D-W equation and fluid properties values from our heat exchanger case evaluated at the average mean bulk temperature.

$$v_1 = \sqrt{\frac{dp \cdot D_i \cdot 2}{\rho_i \cdot \lambda_i \cdot L_1}} = 27.985 \ m/s$$

$$v_2 = \sqrt{\frac{dp \cdot D_i \cdot 2}{\rho_i \cdot \lambda_i \cdot L_2}} = 26.562 \ m/s$$

Different velocities mean different Reynolds numbers (Re) but Prandtl number (Pr) will remain unchanged for both cases.

$$Pr = \frac{\mu_i \cdot cp_i}{k_i} = 0.74$$

$$Re_1 = \frac{v_1 \cdot D_i \cdot \rho}{\mu} = 2.309 \cdot 10^4$$

$$Re_2 = \frac{v_2 \cdot D_i \cdot \rho}{\mu} = 2.192 \cdot 10^4$$

Then we calculate friction factor (f) using Haaland equation [11] and Nusselt number (Nu) using Pethukov equation which is valid for $0.5 \leq Pr \leq 2000$ and $10^4 \leq Re \leq 5x10^6$ [11].

$$f_1 = \sqrt{\frac{1}{-1.8 \cdot log\left[\left(\frac{6.9}{Re_1}\right) + \left(\frac{r}{3.7}\right)^{1.11}\right]}} = 0.45$$

$$f_{12} = \sqrt{\frac{1}{-1.8 \cdot log\left[\left(\frac{6.9}{Re_2}\right) + \left(\frac{r}{3.7}\right)^{1.11}\right]}} = 0.451$$

$$Nu_1 = \frac{Re_1 \cdot Pr \cdot \left(\frac{f_1}{8}\right)}{1.07 + 12.7 \cdot \left(\frac{f_1}{8}\right)^{0.5} \cdot \left(Pr^{\frac{2}{3}} - 1\right)} = 1.854 \cdot 10^3$$

$$Nu_2 = \frac{Re_2 \cdot Pr \cdot \left(\frac{f_2}{8}\right)}{1.07 + 12.7 \cdot \left(\frac{f_2}{8}\right)^{0.5} \cdot \left(Pr^{\frac{2}{3}} - 1\right)} = 1.761 \cdot 10^3$$

From Nusselt number can be calculated heat transfer coefficient (h).

$$h_1 = \frac{Nu_1 \cdot k_i}{L_1} = 67.563 \ \frac{W}{m^2 K}$$

$$h_2 = \frac{Nu_2 \cdot k_i}{L_2} = 57.834 \ \frac{W}{m^2 K}$$

$$\frac{h_1}{h_2} = 1.168$$

It can be seen that heat transfer coefficient for shorter tube is higher of 17 %. To see how this influencing the overall heat transfer we will use thermal resistance concept, which is analogous to electrical circuit problems. R_{total} is total thermal resistance and is composed by thermal resistance of inner convection resistance (R_i), wall resistance (R_w) and outer convection resistance (R_o).

$$\dot{Q} = \frac{\triangle T}{R_{total}}$$

$$R_{total} = R_i + R_w + R_o$$

$$R_{total} = \frac{1}{A_i \cdot h_i} + \frac{ln\left(\frac{D_o}{D_i}\right)}{2 \cdot \pi \cdot k_w \cdot L} + \frac{1}{A_o \cdot h_o}$$

Thermal conductivity of the wall can be find in tables so only unknown is outer heat transfer coefficient. Nusselt number for cross flow over tube banks need to be calculated first. In literature [11] was found Zukauskas equation.

$$Nu_D = C_g \cdot Re_D^m \cdot Pr^n$$

Constant coefficients C_g, m and n can be calculated from staggered tube arrangement dimensions.

$$Nu_D = 45.231$$

$$h_o = \frac{Nu_D \cdot k_o}{D_o} = 74.9 \ \frac{W}{m^2 K}$$

Then it is possible to calculate total thermal resistance for both cases.

$$R_{total,1} = \frac{1}{A_{i1} \cdot h_{i1}} + \frac{ln\left(\frac{D_o}{D_i}\right)}{2 \cdot \pi \cdot k_w \cdot L_1} + \frac{1}{A_{o1} \cdot h_{o1}} = 0.361 \ \frac{K}{W}$$

$$R_{total,2} = \frac{1}{A_{i2} \cdot h_{i2}} + \frac{ln\left(\frac{D_o}{D_i}\right)}{2 \cdot \pi \cdot k_w \cdot L_2} + \frac{1}{A_{o2} \cdot h_{o2}} = 0.371 \ \frac{K}{W}$$

$$\frac{R_{total,2}}{R_{total,1}} = 1.029$$

From the ratio of total thermal resistance is obvious that if tube is shorter by 10 % then it will take 3 % more heat. There are 17 rows of tubes with the same length. If we consider that the middle one (row number 9) is ideal case and its outlets temperature is 340 °C. Then it is possible to determine outlet temperatures of others rows by described calculation procedure. Knowing the new outlet temperatures we can easily calculate others fluid properties influencing inertial resistance coefficient C_2via calculation of addition imaginary length of tube caused by heat transfer. However as can be noticed in Table 18 there is minimal difference between these fluid properties and thus it is not worth to recalculate $C_2$and do another CFD simulation.

Table 18: new assumption

Row number	Total length of straighten tube [m]	Difference between length of tubes in rows and reference row [%]	Calculated outlet temperature [°C]	Calculated density [kg/m^3]	Calculated velocity [m/s]
1	7.008	13	351.56	0.76	14.54
2	7.134	11	349.86	0.77	14.51
3	7.261	9	348.16	0.77	14.48
4	7.387	8	347.14	0.77	14.46
5	7.513	6	345.44	0.77	14.44
6	7.640	5	344.42	0.77	14.42
7	7.766	3	342.72	0.77	14.39
8	7.893	2	341.70	0.77	14.38
9 (ref)	8.019	0	340.00	0.77	14.35
10	8.146	2	338.30	0.78	14.32
11	8.272	3	337.28	0.78	14.31
12	8.398	5	335.58	0.78	14.28
13	8.525	6	334.56	0.78	14.27
14	8.651	8	332.86	0.78	14.24
15	8.778	9	331.84	0.78	14.22
16	8.904	11	330.14	0.78	14.20
17	9.031	13	328.44	0.78	14.17

4.5 Summary

The porous zone approach was applied on the real heat exchanger. Task was to identify why heat exchanger tubes are chocking up in the specific areas. The CFD simulation was done. Formation of vortexes in problematic places and poor flow distribution were identified. The mass flow rate through the middle section was higher by 12.5 % then right section and by 8.6 % then left section. Conclusion was that diffuser is not functioning and it need to be redesign. Therefore the new design of diffuser was created. It is longer and includes 2 rows of baffle. The CFD simulation for the new design was performed. The new results proved better distribution of the flow and no more vortex creation. Now the mas flow rate in right section is the highest and it differs by 2 % from the middle section and by 6 % from the left section. In the next step we run new design heat exchanger simulation with the temperature influence. The temperature influence was implement into porous zone via internal resistance coefficient C_2. There are no big changes compared to previous results. It is because we assumed the same outlet temperature from every tube. Therefore added value of internal resistance coefficient C_2 to each row of tubes with the same length was almost constant. The internal resistance coefficient C_2 kept its linear character caused length of the tubes.

5 Mesh quality influence

5.1 Introduction

As it was found out in section 3.4 mesh quality has a big influence on the results. A very fine grid is usually the best choice but it needs much computational power. Therefore there is an effort to find out how much coarse the mesh could be without loosing too much accuracy in the results. Burner test chamber, which is placed in our laboratory (see Figure 34) will be used for a short insight into this issue. Because there are experimental data from measurements, which can be used for the comparison with our CFD simulation.

Figure 34: Burner test chamber [13]

5.2 Burner test chamber

The burner test chamber is a horizontally situated cylinder with the inner diameter 1 m and an adjustable length from 2 m up to 4 m. Its shell is cooled by circulating water and headings are insulated with isolation, which is 100 mm thick. Due to water cooling it is possible to measure wall heat fluxes. Water cooling system is divided into 7 sections and the water mass flow rate and the temperature is measured at the inlet and at the outlet of each section. This allows us to evaluate local heat flux from the burner into walls of chamber. The chamber is equipped with 8 inspection windows on each side. The distance between 2 windows is 0.5 m. And there are also 2 inspection windows at the heading opposite the burner. Inspection windows are used to observe a flame or for additional installation of measuring instruments such as thermocouples or a radiation probe. The chamber

can operate with sub-atmospheric or super-atmospheric pressure. [13]

5.3 Mesh and solver settings

The model and mesh of the burner test chamber was created in Gambit (see Figure 35).

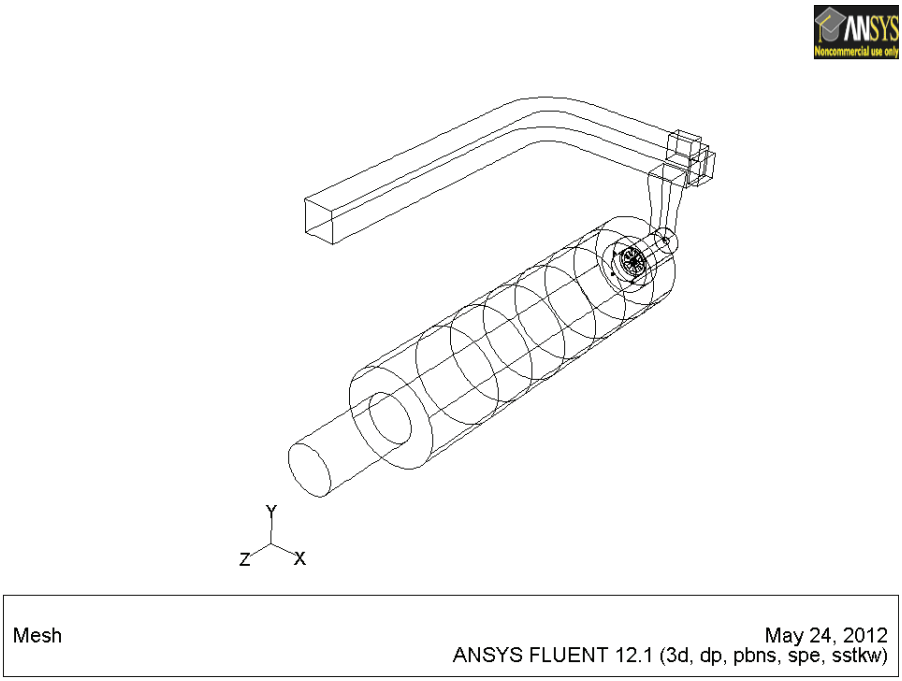

Figure 35: Model of burner test chamber

Mesh has 1 270 668 cells and most of it (97 %) are hexahedral, 2.53 % are tetrahedral and rest are pyramids. This mesh was used before for calculations. The mesh was modified by adding part of flue gas ducting. The reason of this modification was to prevent reverse flow at the outlet from the computational domain. Firstly the calculation was done with this basic mesh. Then we, based on results, adapted cells in a guide vane swirl generator region and flame region aiming at approximately 2 millions cells. A new calculation was done with refined mesh and both results were compared. The mesh adaptation is a way to refine mesh in selected area of large gradients and obtain more precise solution. Fluent is providing many possibilities to help a user to select the correct area. Here we are going to list ones, which are used most. There is the boundary adaption to

refine mesh in the near-wall region, gradient adaption to refine mesh in a region with the largest gradients, region adaption to allow the user pick up a region and isovalues adaption for cases where a region can be identify based on values of a certain quantity (like jets). The selection of the adapted region is based on the results described in the next section. [4]

Utilized turbulence model was k-ω SST with compressibility effects. All elements needed for chemical reaction and air mixture were defined. Mass flow rates at the inlet of air and gas were set according to the measured data (see Table 19 and Figure 36). Pressure-velocity coupling scheme was set SIMPLE and spatial discretization was set to the first order upwind.

Table 19: Boundary conditions

Inlet	Mass flow rate [kg/s]	Temperature [°C]	Composition [% of mass]
air	0.28528	16.5	23 % O_2, 0.05 % CO_2, 0.54 % H_2O, 76.41 % N_2
primary gas 1	0.0015287	19.2	100 % CH_4
primary gas 2	0.0023024	19.2	100 % CH_4
secondary gas	0.0110265	19.2	100 % CH_4

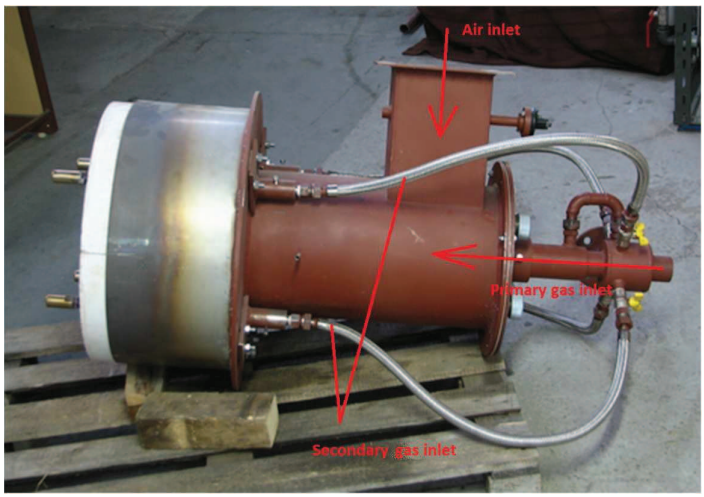

Figure 36: Burner with marked inlets

5.4 Results with basic mesh

The simulation on cluster server took a very long time due to complexity of the task. Divergence problem appeared an therefore initial values had to be assigned separately into the domain of combustion air duct and chamber itself. Also solver equations were added step by step (flow, turbulence, species, energy and radiation). At first we used only flow and turbulence equation, then we added species equation followed by energy equation and radiation equation. This step by step procedure paid off and calculation was stable.

The results were obtained and plotted. In Figure 37 can be observed contours of velocity and contours of temperature.

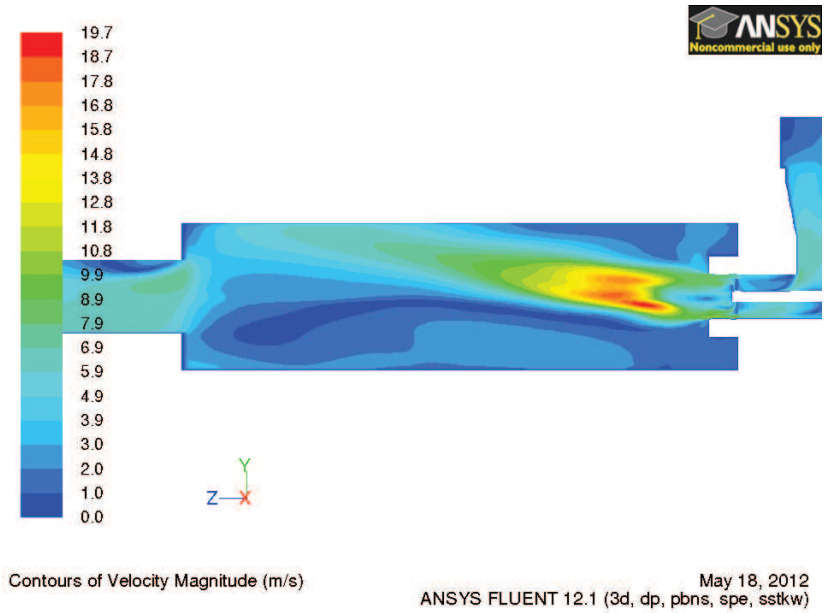

(a) Contours of velocity

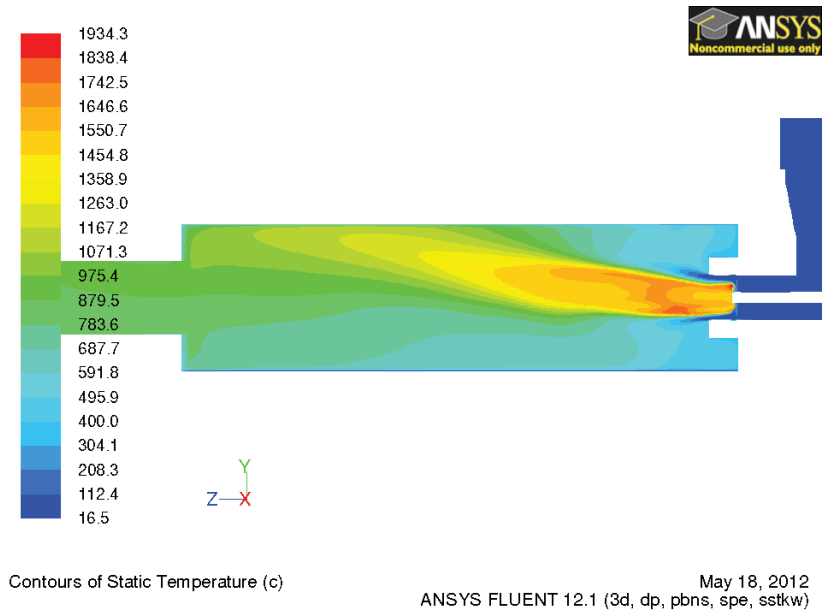

(b) Contours of static temperature

Figure 37: Results

Notice that the region of the highest gradients is almost the same for both cases. Therefore there should be the finest mesh in order to obtain more precise results. To achieve this condition we used adapt mesh function and chose cells for adapting by isovalues of temperature (1700 °C - 1935 °C) and region defined by coordinates. The region defined by coordinates was placed around guide vane swirl generator, because high turbulence intensity is expected behind these geometry. The region defined by isovalues of temperature were chosen to refine area in the flame. In Figure 38 both regions can be seen clearly. It may seem to be a poor number of cells for adapting but after adapting procedure total cell amount is 2.1 million. This is a big growth from the basic mesh with 1.2 million cells.

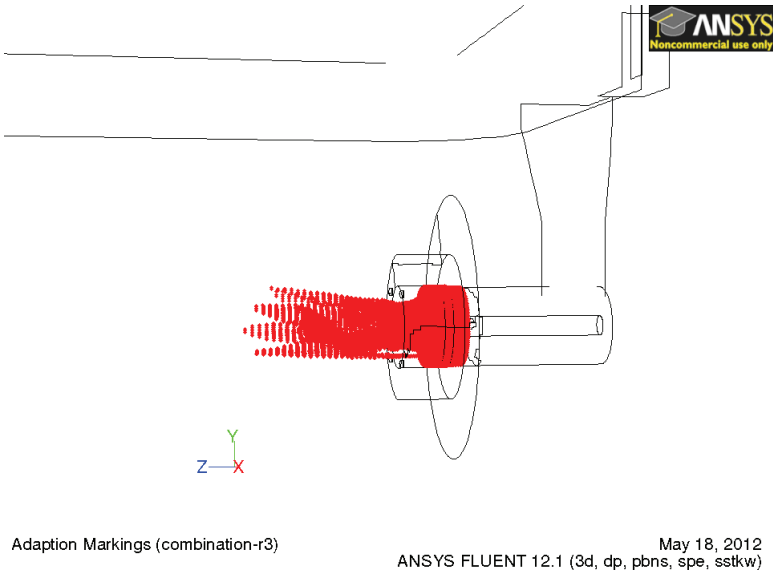

Figure 38: Marked cells

In the Figure 39 can be seen comparison between measured and simulated heat flux to the chamber wall. It can be noticed that computed results are in a good agreement with measured data. We would like to confirm grid independence with adapted mesh. The calculation procedure were repeated with the same settings.

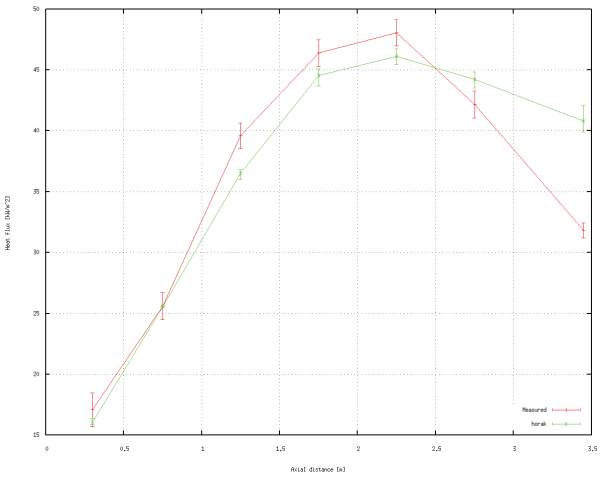

Figure 39: Comparison of measured and computed heat flux

5.5 Results with adapted mesh

Even thought the basic mesh was in a good agreement with the measured data it was decided to test grid independence on adapted mesh. However calculation with refined mesh appeared to be beyond the scope of this thesis. The number of cells were doubled but expected solution time was 15 times longer. The results reached so far can be seen in Figure 40 where are compared heat fluxes calculated with the adapted mesh and with the basic mesh. We already know that the results with the basic mesh were in a good agreement with measured data. Therefore we are expecting the similar behavior of heat fluxes in a case with adapted mesh. But if we compare both figures then it is clear that simulation with adapted mesh is not going well so far.

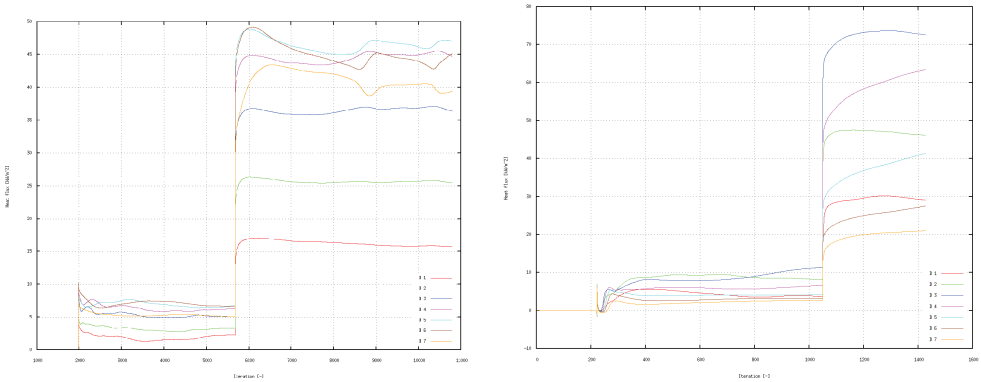

(a) basic mesh **(b)** adapted mesh

Figure 40: Heat fluxes monitors in individual sections

As can be seen from Figure 42 the flame is split in the middle and heading up and down, further investigation showed that it is also heading to the left and to the right. This explains why the heat flux was so intense to the third and fourth section.

The explanation might be that the wrong region for adaptation was selected. The mesh is of low quality which causes numerical error (see Figure 41). Another reason might be that calculation has not converged yet. This assumption is based on Figure 42. It shows the low velocity region on the axis of the chamber in flue gas duct. This velocity profile is unrealistic.

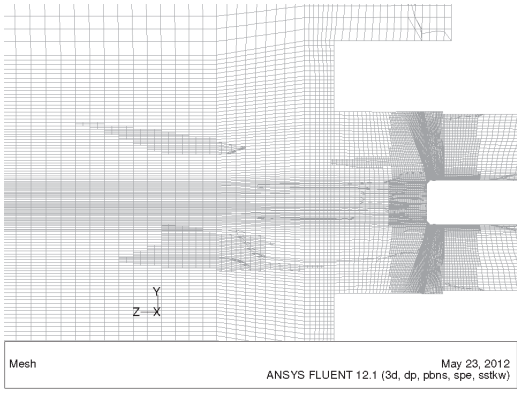

Figure 41: Adapted mesh

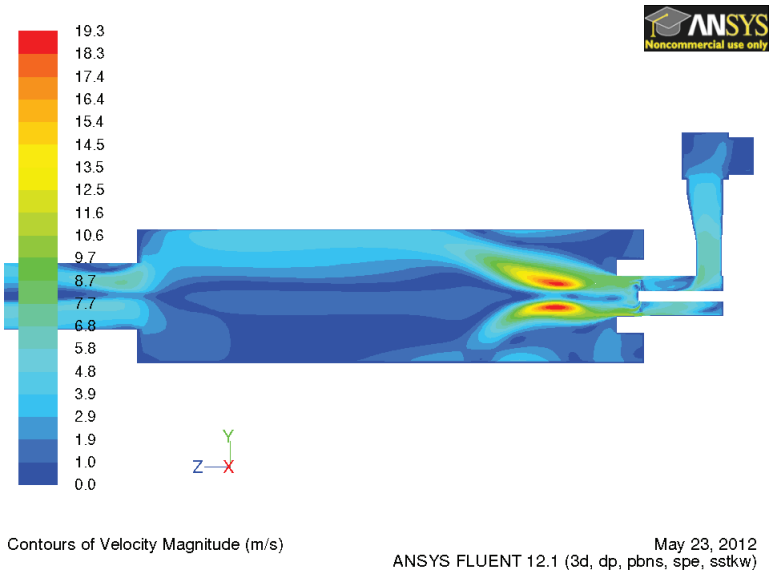

(a) Contours of static velocity

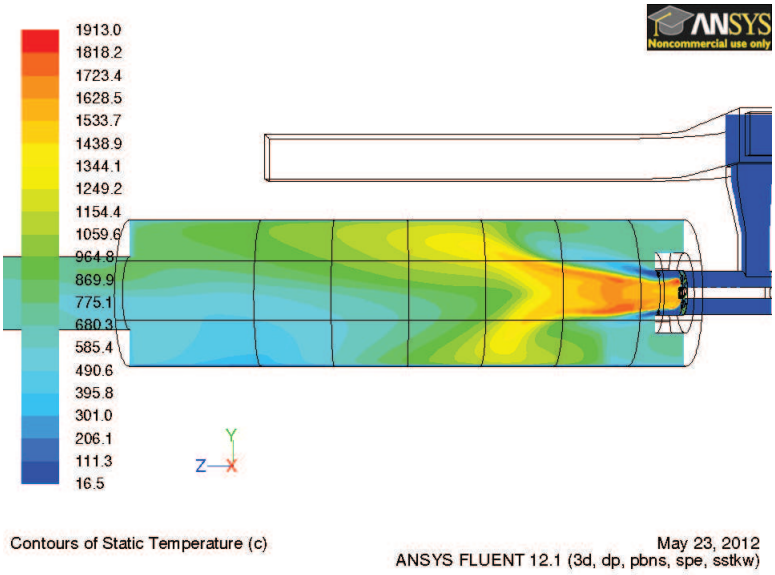

(b) Contours of static temperature

Figure 42: Results with adapted mesh

6 Conclusions

The possibility to simplify geometry used by CFD, when dealing with large scale heat exchangers was studied. The idea of simplification was to replace major part of heat exchanger tubes by porous zone. The motivation was the large heat exchanger with chocking problems. Therefore CFD simulation had to be performed to identify what is causing these problems. U-tube from this heat exchanger was modeled and CFD simulation was done to investigate the pressure drop. The major part of U-tube was replaced by the porous zone. The porous zone performance was defined by internal resistance coefficient C_2, which was calculated from the replaced length of the U-tube and length of the porous zone. The porous zone tube was again modeled and run through CFD analysis. It turned out that turbulence model and mesh has big influence on the result. The best choice was realizable k-ε turbulence model with standart wall functions. Mesh was created based on turbulence model specification with Y+ value of 35. The difference between pressure drop of the U-tube and the tube with porous zone was 4 %. This difference was acceptable and we applied porous zone concept on the whole heat exchanger and performed CFD simulation. The results revealed poor performance of diffuser and vortex formation. The difference between maximum and minimum mass flow rate between rows of tubes was 25 %. The highest mass flow rate was going through the middle section. Vortex formation were located on the same places where were the main chocking problems. A new design of diffuser with two rows of baffle was verified. The new design of diffuser was longer and the first row of baffle should reduce the effect of main pipe bending and the second row of baffle should prevent vortex creation. CFD simulation was run with this new design. The flow distribution was better and there were no more vortexes. The difference between maximum and minimum mass flow rates between rows of tubes was 14 %. This was improvement when compared to previous case. But first row of baffle was instead of reducing effect bending of the main pipe enhancing it. The highest mass flow rate was going through the left section. To reach even better performance we recommend to redesign first row of baffle. The effect of the heat transfer to pressure drop and flow was also investigated. Several ways how to simplify the heat transfer in order to save computational power were simulated. In the end it turned out that the most effective way is to implement temperature influence directly into porous zone via inertial resistance coefficient C_2. With that solution was deviation from full length U-tube with constant heat flux 7 %. This solution was applied on heat exchanger with the new diffuser design and inertial resistance coefficients were changed. The CFD simulation was done again but the

results were almost the same. The reason was that the increase of pressure drop due to temperature influence was almost identical for all the tubes.

The grid independence study was performed on model of combustion chamber. Even though the results of CFD simulation were in a good agreement with measured data, adaptation function was used to refine mesh. The mesh region around guide vane swirl generator was refined. Also the region chosen by isovalues of temperature to cover highest gradients in the flame was refined. The CFD simulation was run again with adapted mesh and we expected results to be closer to measured data. It turned out that the simulation was 15 times more time demanding and therefore it was beyond the scope of this thesis. Preliminary results showed that mesh adaptation predicts higher wall heat fluxes with higher deviations from measurement then in previous case. The possible explanation was that adaptation region was badly selected.

References

[1] MISSIRLIS, D., S. DONNERHACK, O. SEITE, C. ALBANAKIS, A. SIDERIDIS, K. YAKINTHOS a A. GOULAS. Numerical development of a heat transfer and pressure drop porosity model for a heat exchanger for aero engine applications. Applied Thermal Engineering. 2010, vol. 30, 11-12, p. 1341-1350. ISSN 13594311. DOI: 10.1016/j.applthermaleng.2010.02.021. Available from: http://linkinghub.elsevier.com/retrieve/pii/S1359431110000803

[2] SHI, Yu-Ling, Jun-Jie JI a Chun-Lu ZHANG. Semiporous Media Approach for Numerical Simulation of Flow through Large-Scale Sparse Tubular Heat Exchangers. HVAC. 2010-9-1, vol. 16, iss. 5, p. 617-628. ISSN 1078-9669. DOI: 10.1080/10789669.2010.10390924. Available from: http://www.informaworld.com/openurl?genre=article

[3] WANG, Yuan, Matthew BRANNOCK, Shane COX a Greg LESLIE. CFD simulations of membrane filtration zone in a submerged hollow fibre membrane bioreactor using a porous media approach. Journal of Membrane Science. 2010, vol. 363, 1-2, p. 57-66. ISSN 03767388. DOI: 10.1016/j.memsci.2010.07.008. Available from: http://linkinghub.elsevier.com/retrieve/pii/S0376738810005442

[4] FLUENT, Fluent 12.1 User's Guide, FLUENT, Lebanon

[5] ERTESVÅG, Ivar. Turbulent Flow and Combustion. Trondheim: NTNU, 2008

[6] ASLAM BHUTTA, Muhammad Mahmood, Nasir HAYAT, Muhammad Hassan BASHIR, Ahmer Rais KHAN, Kanwar Naveed AHMAD a Sarfaraz KHAN. CFD applications in various heat exchangers design: A review. Applied Thermal Engineering. 2012, vol. 32, p. 1-12. ISSN 13594311. DOI: 10.1016/j.applthermaleng.2011.09.001. Available from: http://linkinghub.elsevier.com/retrieve/pii/S1359431111004807

[7] ŠOB, František. Hydromechanika: studijní materiál pro I. stupeň magisterského studia, 2. a 3. ročník. Brno: Akademické nakladatelství CERM s.r.o., 2002, 238 pages. ISBN 80-214-2037-5.

[8] ŠTEFAN, David. Hydraulické ztráty v potrubí. Brno, 24.11.2008. Bakalářská práce. VUT. Vedoucí práce Ing. Pavel Rudolf, Ph.D.

[9] The Engineering ToolBox. [online]. [cit. 2012-04-13]. Available from: http://www.engineeringtoolbox.com/air-properties-d_156.html

[10] BUREŠ, Jiří. ConVERTER: conVERTER je web zaměřený na převody jednotek, fyzikální tabulky, životopisy fyziků a informace o Nobelově ceně. [online]. [cit. 2012-04-14]. Available from: http://www.converter.cz/tabulky/vzduch.htm

[11] ÇENGEL, Yunus A. Heat and mass transfer: a practical approach. 3rd ed. Boston: McGraw-Hill, c2007, 901 s. McGraw-Hill series in mechanical and aerospace engineering. ISBN 978-007-3250-359.

[12] SHAH, Ramesh K. Fundamentals of heat exchanger design. New York: John Wiley, 2003, 941 s. ISBN 0-471-32171-0.

[13] ÚPEI: VUT Brno. [online]. [cit. 2012-04-26]. Available from: http://www.upei.fme.vutbr.cz/veda-vyzkum/experimentalni-zakladna-zkusebna-horaku